



2D BioPAD

Supple Graphene Bio-Platform for
point-of-care early detection and
monitoring of Alzheimer's Disease

D2.1 Conjugated MNPs/Aptamers Design, Synthesis and Selection Version1

AUTh

30/09/2024

Document Information



Funded by
the European Union

Issued by:	AUTH
Issue date:	30/09/2024
Due date:	30/09/2024
Work package leader:	AUTH
Dissemination level:	SEN

Document History

Version	Date	Modifications made by
0.1	31/07/2024	Table of Contents provided by AUTH
0.2	01/09/2024	First draft with input from partners circulated for initial comments by AUTH
0.7	24/09/2024	Final draft circulated for Review by AUTH
0.7	27/09/2024	Quality Review by ICN2 and UEF
1.0	30/09/2024	Final version for submission

Authors

Name(s)	Beneficiary
M. Angelakeris M., A. Pantazaki	AUTH
J.J. Toulmé, S. Kumar S.	Novaptech
C. Bosch, P. Goktas	CeADAR, UCD

In case you want any additional information, or you want to consult with the authors of this document, please send your inquiries to: agelaker@auth.gr

Quality Reviewers

Name(s)	Beneficiary
Marianna Rossetti	ICN2
Alina Solomon	UEF

Disclaimer

Funded by the European Union under GA no. 101120706. Views and opinions expressed are however those of the authors only and do not necessarily reflect those of the European Union or CNECT. Neither the European Union nor the granting authority can be held responsible for them.

© 2D-BioPAD Consortium, 2024

Reproduction is authorised provided the source is acknowledged.

Executive Summary

This report, developed within the 2D-BioPAD project funded by the European Union's Horizon Europe Framework Programme for Research and Innovation 2021-2027, outlines the activities and findings related to Task 2.1: Identification, synthesis, and evaluation of Aptamers for AD protein biomarkers and Task 2.3: Synthesis and characterisation of magnetic nanoparticles (MNPs) as carriers and enablers (M4-M24) under Work Package 2 (WP2): Biomarkers binding and quantitative analysis running from M4 (January, 2024) to M30 (March, 2026). WP2 also includes Task 2.2: Optimization and functionalisation of aptamers (M13-M24) and Task 2.4: Immobilization, Functionalization and Evaluation of Conjugated MNPs/Aptamers/Biomarkers (M18-M30).

The primary goal of WP2 is provide standardized nano-based probes for reliable, efficient, and ethical early diagnosis of AD. This includes the following objectives:

- ✓ *Objective 2.1. Identification, synthesis, functionalisation, and optimisation of DNA aptamers for AD protein biomarkers.*
- ✓ *Objective 2.2. Identification, synthesis, characterisation, and evaluation of MNPs as carriers and enablers.*
- ✓ *Objective 2.3. Conjugation of aptamers, MNPs, and Biomarkers with AD protein biomarkers.*
- ✓ *Objective 2.4. Evaluation and validation of individual and conjugated components.*

Within this reporting period, Task 2.1 initiated and is still running to identify certain DNA aptamers for specific AD protein biomarkers, namely five different AD biomarker proteins viz. A β 40, A β 42, NF-L, GFAP and p-tau 217, as defined and explained in D1.2 Architecture and System Design.¹ Task 2.2 will initiate once Task 2.1 becomes conclusive regarding threshold identification of DNA aptamers. Task 2.3 provides already different formulation of MNPs to be checked for effective conjugation with selected aptamers of Task 2.1. Task 2.4 is currently underway with reference specimens to provide a rigorous framework for future experimental sequences.

Objective 2.1 is underway for A β 40, A β 42 peptides, Tau proteins phosphorylated at specific sites, GFAP and NFL with respect to identification and characterization. Synthesis of DNA aptamers for the corresponding AD protein biomarkers will take place after this reporting period when Task 2.2 will initiate.

Objective 2.2 is fulfilled concerning the synthesis of MNPs while characterization is in progress and expected to conclude within next reporting period.

Objective 2.3 is directly connected to Task 2.2 and expected to be fulfilled by the end of WP2.

Objective 2.4 is underway concerning MNPs (Task 2.3) while preliminary results for aptamers (Task 2.4) are already running to establish a rigorous protocol for the specific DNA aptamers for AD protein biomarkers.

¹ D1.2 was submitted on 2nd July 2024.

Table of Contents

EXECUTIVE SUMMARY	2
1. INTRODUCTION	7
1.1 THE PROBLEM	7
1.2 THE 2D-BIOPAD APPROACH	8
1.3 THE 2D-BIOPAD FRAMEWORK	10
1.4 BIOMARKERS BINDING: THE ROLE OF APTAMERS AND NANOPARTICLES	11
1.5 BIOMARKERS BINDING: QUANTITATIVE ANALYSIS	14
2. CONJUGATION DESIGN, SYNTHESIS, AND SELECTION	16
2.1 APTAMERS' IDENTIFICATION	18
2.2 APTAMERS' SELECTION	23
2.3 NANOPARTICLES' DESIGN & SYNTHESIS	31
2.4 CONJUGATION OF NPs WITH APTAMERS	35
2.5 FUTURE STEPS	41
3. INTERACTIONS	43
4. CONCLUSIONS	45

List of Figures

Figure 1: Global AD evolution statistics.....	7
Figure 2: Main user needs, challenges and PoC IVDs requirements for AD as concluded in D1.1.....	8
Figure 3: 2D-BioPAD system concept.....	10
Figure 4: Overview of 2D-BioPAD AD biomarkers.....	12
Figure 5: a) Schematic illustration of an MNP conjugated with an aptamer b) Illustration of the optimum scenario, one 1 MNP ↔ 1 aptamer ↔ 1 biomarker including 4 steps: Before conjugation, During conjugation, Immobilization and detection.....	14
Figure 6: Schematic outline of Work Package 2: Biomarkers binding and quantitative analysis.....	16
Figure 7 Details underlying the iterative forward sampling algorithm using MCTS to generate aptamer sequences ⁹⁷	21
Figure 8: SPR sensorgrams obtained for literature aptamers with Aβ peptides.....	24
Figure 9: Binding/affinity evaluation of literature aptamer Aβ-apt with Aβ ₄₀ peptides by BLI. The responses are maroon- 1000 nM, blue 500 nM, green 250 nM, and orange is 125 nM. Continuous lines correspond to curve fittings.....	25
Figure 10: Processed data showing the binding signals after background subtraction. The different lines are- the maroon line- 0 nM, aqua line- 1000 nM, green line 500 nM, orange line 250 nM, and blue line indicates 125 nM of Aβ ₄₂ peptide. Here the negative graphs were obtained because background binding was subtracted it was higher than binding with aptamer.....	25
Figure 11: Evolution of the pool from R06 to R10.....	27
Figure 12: Percent T and C composition of selection round 10 for conditions A and B. For comparison, the starting aptamer library compositions for both conditions have been shown as R00A and R00B.....	28
Figure 13: Sensorgrams obtained for the interaction between the different oligonucleotide candidates and GFAP. The three libraries (Bq) used for the selection were used as references.....	30
Figure 14: SPR analysis of the interaction between candidates FIB002B and FIB007A.....	30
Figure 15: Left figure: X-ray Diffraction (XRD) pattern of the synthesized nanoparticles. Right figure: (top): Transmission Electron Microscopy (TEM) image showing agglomerates of magnetic nanoparticles (MNPs), specifically Fe ₃ O ₄ , with gold nanoparticles (Au NPs) decorating their surface, forming an inositol hexaphosphate (IP6) network. (Center and Bottom): TEM images of core-shell nanoparticles, with Fe ₃ O ₄ as the core and Au as the shell (Fe ₃ O ₄ @Au NPs).....	32
Figure 16: Dynamic Light Scattering (DLS) of Au decorated MNPs (a), core/shell (c), Au reference (e), and ζ-potential analysis of the synthesized nanoparticles (b), (d) and (f) respectively.....	33
Figure 17: Hysteresis loop of Au-Fe ₃ O ₄ nanoparticles: Au decorated MNPs (grey) and core/shell NPs (blue), as measured by Vibrating Sample Magnetometry (VSM).....	34
Figure 18: (a) 6-Carboxyfluorescein (FAM)-modified thrombin aptamer solutions in Tris-EDTA (TE) buffer (From left to right: 0.6, 0.9, 1.19, 2.34, 4.69 μM). (b) Standard curve of the fluorescence of FAM-modified aptamers (Excitation 490 nm, emission 510-570 nm).....	36
Figure 19: (a) Suspensions of Au NPs after freeze-thaw treatment, in the absence (far left tube) or presence of various concentrations of thrombin aptamer (From left to right: 0.60, 0.89, 1.19, 1.77, 2.34 μM). (b) Stability of AuNPs with freeze-thaw treatment in the absence or presence of aptamer, after 2 hours and 14 days. (c) The ratio of the absorbance of AuNPs' suspensions at 520 nm versus the one at 650 nm, before (w/t) and after (w) freeze-thaw treatment, and in the presence of several thrombin aptamer concentrations (0.60, 0.9, 1.19, 1.77, 2.34, 3.47 μM). (d) Agarose (0.8% w/v) electrophoretic analysis of AuNPs after freeze-thaw treatment in the absence or presence of various thrombin aptamer concentrations. (e) Number of thrombin aptamer molecules per AuNP after freeze-thaw treatment, detachment of aptamers with DTT and fluorometric analysis of 6-FAM. The concentration of the detached aptamers was calculated from a fluorescence standard curve (Figure 18:b).....	37
Figure 20: (a) Agarose (0.8% w/v) electrophoretic analysis of thrombin aptamer-Au NP nanoconjugates, in the absence or presence of 5 μg of thrombin (b) SDS-Polyacrylamide gel (10%, w/v) electrophoretic analysis of thrombin detached from aptamer-AuNP nanoconjugates, after overnight staining with Blue Silver stain. (c) An	

indicative thrombin quantity is also run in lane 2 for proof of concept. The bands' intensity was semi-quantified with ImageJ software..... 38

Figure 21: (a) Suspensions of core/shell NPs after freeze-thaw treatment, in the absence (far left tube) or presence of various concentrations of thrombin aptamer (From left to right: 0.60, 1.19, 2.34, 3.47 μM). (b) Bound thrombin aptamer on core/shell NPs after freeze-thaw treatment, detachment of aptamers with DTT, and fluorometric analysis of 6-FAM. The concentration of the detached aptamers was calculated from a fluorescence standard curve (Fig. 1b). (c) Agarose (0.8% w/v) electrophoretic analysis of thrombin aptamer-core/shell NP nanoconjugates, in the absence or presence of 5 μg of thrombin (1->11: pure core-shell Au NPs; core-shell Au NPs with 0.60, 1.19, 2.34, 3.47 μM of TBA1 aptamer; core-shell Au NPs with 0.60, 1.19, 2.34, 3.47 μM of TBA1 aptamer, and after incubation with 5 μg of thrombin). 40

List of Tables

Table 1: Terms and Definitions.	6
Table 2: Evaluation of Functionalities, Limitations, and Suitability of Computational Aptamer Binding Research Methodologies including MLPD, RaptGen, AptaNet, APIPred, AptaBERT, AptaTrans, and Apta-MCTS.....	20
Table 3: Literature Aptamers for AD protein biomarkers.....	24
Table 4: Sequences for biophysical characterisation after selection against GFAP.	29
Table 5: Nanoparticle formulations composed of Au/Fe ₃ O ₄ synthesized within WP2 framework and the corresponding synthetic methodologies.	31
Table 6: Overview of the aptamer-nanoparticle conjugation	40

List of Terms and Definitions

Table 1: Terms and Definitions.

Abbreviation	Definition	Abbreviation	Definition
A β	Amyloid Beta	IPR	Intellectual Property Rights
AD	Alzheimer's Disease	IVD	In-Vitro Diagnostics
ADNI	Alzheimer's Disease Neuroimaging Initiative	IVDR	In-Vitro Diagnostics Regulation
AI	Artificial Intelligence	KER	Key Exploitable Result
APOE	Apolipoprotein E gene	LFA	Lateral-flow biosensor assays
"ATN"	Research framework which covers amyloid abnormalities ('A'), tau protein changes ('T'), and evidence of neurodegeneration ('N'), irrespective of clinical phenotypes	LMICs	Low-and middle-income countries
BBBM	Blood-based Biomarker	LOD	Limit of Detection
BRU	Brain Research Unit at UEF	MCI	Mild Cognitive Impairment
CIS	Clinical Information System	MDR	Medical Device Regulation
CSF	Cerebrospinal fluid	MNPs	Magnetic Nanoparticles
D	Deliverable	MRI	Magnetic Resonance Imaging
DFT	Density-functional theory	NACC	National Alzheimer's Coordinating Center
DMP	Data Management Plan	NFL	Neurofilament Light
DNA	Deoxyribonucleic acid	NIA-AA	National Institute on Aging and Alzheimer's Association
DNS	Digital Neuro Signature	NPs	Nanoparticles
EC	European Commission	NTA-tau	N-terminal containing tau fragments
ECR	Ethical Consideration Roadmap	PCR	Polymerase chain reaction
EDC	Electronic Data Capture	PDB	Protein Data Bank
ELISA	Enzyme-linked immunosorbent assay	PET	Positron emission tomography
ePADs	Electrochemical paper-based analytical devices	PhD	Philosophy Doctorate
ESC	Ethics Steering Committee	PoC	Point-of-Care
EU	European Union	Post-Doc	Post Doctoral
FAIR	Findable, Accessible, Interoperable and Re-usable	PPIE	Patient and Public Involvement and Engagement
FDG	Fluorodeoxyglucose	RNA	Ribonucleic acid
FG	Fluorographene	QA	Quality Assurance
GAAIN	Global Alzheimer's Association Interactive Network	QC	Quality Control
GCP	Good Clinical Practice	QoL	Quality of Life
GDPR	General Data Protection Regulation	RWE	Real World Evidence
GFAP	Glial Fibrillary Acidic Protein	SELEX	Systematic Evolution of Ligands by Exponential Enrichment
GFET	Graphene field effect transistor	SCI	Subjective Cognitive Impairment
GGC	Greenlight Guru Clinical	SOP	Standard operating procedure
GMP	Good Manufacturing Practice	sTREM2	Soluble triggering receptor expressed on myeloid cells 2
GP	General practitioner	tau	Tau protein
HCPs	Healthcare Professionals/Practitioners	TDP-43	TAR DNA-binding protein 43
HICs	High-income countries	WMA	World Medical Association
hPSCreg	Human Pluripotent Stem Cell Registry	WP	Work Package

1. Introduction

1.1 The Problem

Alzheimer's disease (AD) is a progressive and irreversible neurodegenerative disorder that primarily affects the elderly population. It is the most common cause of dementia, accounting for approximately 60-80% of all cases,^{2,3 4} and affecting over 1 in 9 people aged 65 and older. By 2050, it is expected to impact about 18.8 million people in Europe,⁵ creating a significant financial burden on healthcare, long-term care, and hospice services. The incidence and mortality rates of AD have increased by 145.2% from 2000 to 2019, and this trend is expected to worsen due to population aging as outlined in **Figure 1**.

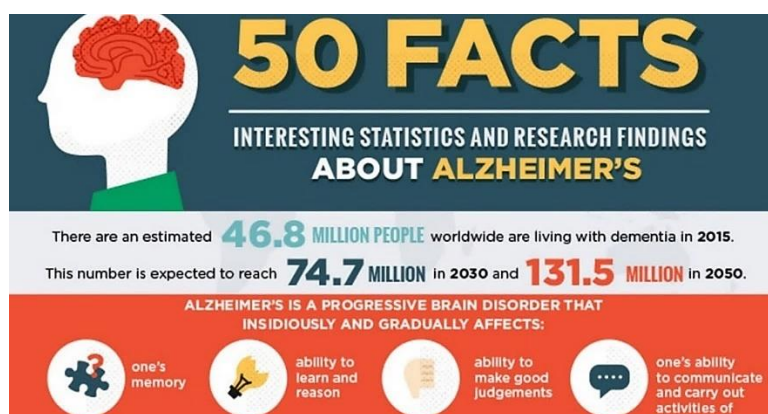


Figure 1: Global AD evolution statistics.

AD is characterized by a gradual decline in cognitive function, including memory loss, language impairment, and reduced ability to perform daily activities.^{6,7}

As the disease progresses, individuals with AD may also experience changes in mood and behavior, including depression, anxiety, and aggression.⁸ The time required for the progression of these symptoms is determined by factors such as age, genetic inheritance, and gender.⁹

The fundamental neuropathological features of AD were initially described in 1906 by Alois Alzheimer and Oscar Fischer.¹⁰ At the macroscopic level, there is brain atrophy. Microscopically, the pathological characteristics of AD include the accumulation of beta-amyloid (A β) plaques and neurofibrillary tangles (NFTs) of tau protein in the brain, leading to the loss of neurons and synapses and subsequent cognitive decline.¹¹ Therefore, it is crucial to address AD at the presymptomatic earlier stages,¹² before the occurrence of substantial impairment.¹³

² Abubakar, M.B. et al., [Alzheimer's Disease: An Update and Insights Into Pathophysiology](#) Front. Aging Neurosci. 14, 1–16 (2022).

³ Coyle, H. et al., [Computerized and virtual reality cognitive training for individuals at high risk of cognitive decline: Systematic review of the literature](#) Am. J. Geriatr. Psychiatry. 23, 4, 335-359 (2015).

⁴ <https://www.alz.org/media/documents/alzheimers-facts-and-figures.pdf>

⁵ <https://www.alzheimer-europe.org/dementia/prevalence-dementia-europe>

⁶ Burns, A., Iliffe, S., [Dementia](#), BMJ, 338 (2009).

⁷ Petersen, R.C., [Mild cognitive impairment: Current research and clinical implications](#). Semin. Neurol. 27(1):22-31 (2007).

⁸ Lyketsos, C.G. et al., [Neuropsychiatric symptoms in Alzheimer's disease](#), Alzheimer's & Dementia 7 532–539 (2011).

⁹ Vermunt, L. et al., [Duration of preclinical, prodromal, and dementia stages of Alzheimer's disease in relation to age, sex, and APOE genotype](#), Alzheimer's & Dementia 15, 888-898 (2019).

¹⁰ Goedert, M., [Oskar Fischer and the study of dementia](#). Brain, 132, 4, 1102–1111 (2009).

¹¹ Hardy, J., Selkoe, D.J., [The amyloid hypothesis of Alzheimer's disease: Progress and problems on the road to therapeutics](#), Science 297, 5580 353-356 (2002).

¹² Gunes, S. et al., [Biomarkers for Alzheimer's Disease in the Current State: A Narrative Review](#). Int. J. Mol. Sci. 23(9), 4962 (2022).

¹³ Albert, M.S. et al., [The diagnosis of mild cognitive impairment due to Alzheimer's disease: Recommendations from the National Institute on Aging-Alzheimer's Association workgroups on diagnostic guidelines for Alzheimer's disease](#). Alzheimer's & Dementia 7, 270–279 (2011).

1.2 The 2D-BioPAD Approach

The 2D-BioPAD project aims to develop a cost-effective, non-invasive point-of-care/self-testing tool for early and accurate prognosis of AD, focusing on early stages like SCI and MCI. Work Package 1 (WP1) of 2D-BioPAD, titled “Requirements & System Architecture” involves analyzing current needs and solutions, creating design guidelines, and co-designing the system’s requirements and architecture.

To address ethical considerations, 2D-BioPAD project, created an Ethical Consideration Roadmap (ECR). The ECR outlines ethics management principles, actions, and responsibilities to ensure compliance with ethical standards.¹⁴

The investigation carried out in the framework of 2D-BioPAD demonstrated that the situation in Europe is highly diverse in terms of clinical needs and processes (**Figure 2**). AD care practices in Finland, Germany, and Greece (the three national Alzheimer’s organizations participating in 2D-BioPAD) differ based on their healthcare systems.

■ Elements identified only in the Semi-Structured Interviews ■ Elements identified only in the Online Survey

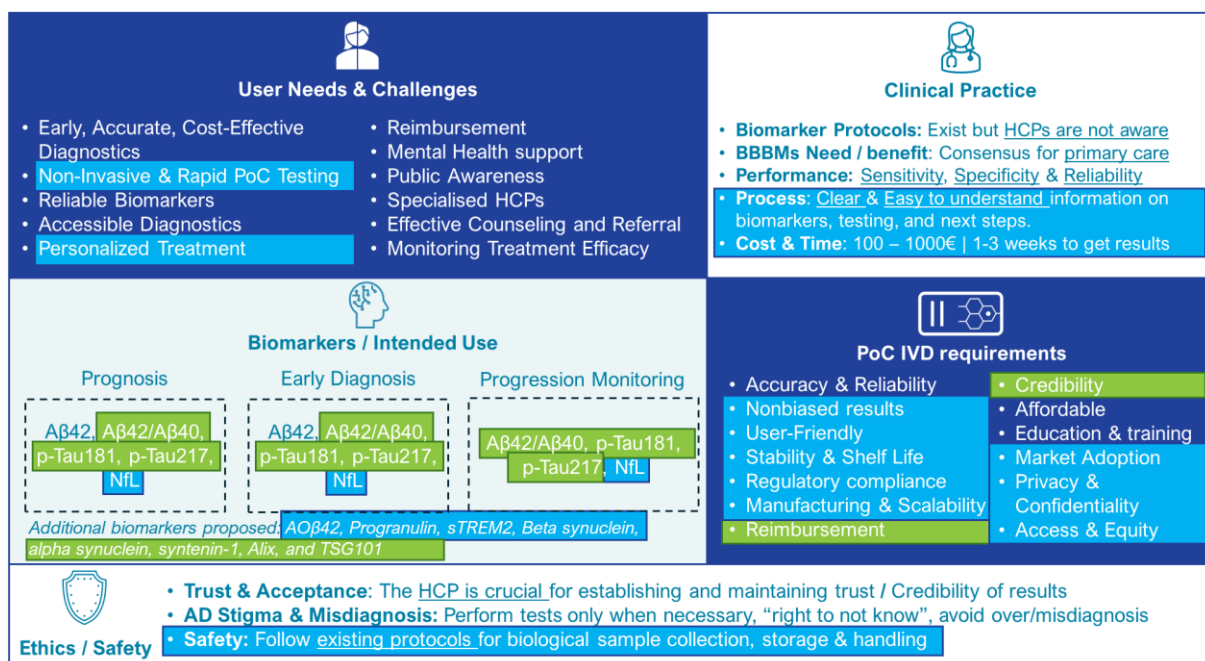


Figure 2: Main user needs, challenges and PoC IVDs requirements for AD as concluded in D1.1.

Despite comprehensive diagnostic capabilities, biomarker-based methods are underutilized due to inadequate reimbursement, leading to diagnostic timelines of up to 1.5 years. In Greece, cognitive issues are usually noticed late, prompting visits to specialized neurologists. However, with the adoption of national dementia strategies and new AD medicines pending EMA approval, decision-making may shift to regional or national levels. This change requires additional data like cost-benefit analyses and health technology assessments, potentially delaying the adoption of new diagnostic systems.¹⁵ Healthcare professionals currently have the flexibility to choose tests and biomarker measurements for patients, but this may change with new medicines and policies. Despite this

¹⁴ The complete ECR is publicly available on the 2D-BioPAD website ([here](#)).

¹⁵ Jönsson, L. et al., [The affordability of lecanemab, an amyloid-targeting therapy for Alzheimer's disease: an EADC-EC viewpoint](#) The Lancet Regional Health–Europe, 29. (2023).

flexibility, primary healthcare providers often misdiagnose 50-70% of patients with AD symptoms, while specialized healthcare providers misdiagnose 25-30%.¹⁶

Therefore, challenges and barriers in diagnosing AD are numerous.¹⁷ Diagnosing AD is complex, particularly in the early stages, with a high risk of misdiagnosis¹⁸ and unnecessary treatments.¹⁹ The cost of diagnostics, especially advanced tests like PET scans and MRIs, is prohibitive for many, posing a significant barrier.²⁰ Recent studies suggest that the use of plasma biomarkers (i.e., p-Tau217) could avoid approximately 57% of PET scans needed for selecting the appropriate treatment option, potentially reducing costs and improving accessibility.²¹ The diagnostic process is also time-intensive, with long waits for diagnostic results and follow-ups. Clinical heterogeneity and lack of standardized practices further complicate diagnosis and research, as does the lack of digital interoperability, which hampers data sharing and collaboration. The aging population exacerbates these challenges,²² increasing demand for dementia diagnostics and straining unprepared primary healthcare systems.²³

In 2014, Kiddle et al. reviewed 163 candidate blood biomarkers for AD and replicated 94, but only 9 were associated with AD phenotypes.²⁴ Despite extensive research, no blood biomarkers have been validated and clinically approved for widespread use. Since 2018, validated AD biomarkers, such as CSF concentrations of A β 42, the A β 42/A β 40 ratio, total tau (t-tau), and p-Tau181, have been introduced into clinical practice.²⁵ MRI is increasingly used for differential diagnosis, yet these biomarkers are not sufficient alone for confident AD diagnosis or disease progression prediction, and should be part of a comprehensive clinical assessment.²⁶ While PET and CSF biomarkers are common in research, they are not routinely used in clinical care for most patients with cognitive decline due to high costs, limited accessibility, and invasiveness. Therefore, 2D-BioPAD refined a specific list of potential blood-based biomarkers as promising, convenient, cost-effective, and less invasive alternatives,²⁷ following a clinical care pathway to address various needs, challenges, and barriers in AD management including

- *Early detection of AD onset (e.g., SCI or MCI) at primary healthcare;*
- *Differential diagnosis and treatment selection at specialized care;*
- *Monitoring treatment response and disease progression at specialized care.*

¹⁶ Hansson, O. et al., [Blood biomarkers for Alzheimer's disease in clinical practice and trials](#) Nature Aging, 3(5), 506-519 (2023).

¹⁷ <https://www.alzint.org/reports-resources/>

¹⁸ Boustani, M. et al., [Implementing a screening and diagnosis program for dementia in primary care](#) Journal of general internal medicine, 20(7), 572-577 (2005).

¹⁹ Howard, R., & Schott, J., [When dementia is misdiagnosed](#) International Journal of Geriatric Psychiatry, 36(6), 799-801 (2021).

²⁰ Depends greatly on the equipment, e.g., 1T vs 3T MRI, etc.

²¹ Mattsson-Carlgen, N. et al., [Plasma biomarker strategy for selecting patients with Alzheimer disease for anti-amyloid immunotherapies](#) JAMA neurology, 81(1), 69-78 (2024).

²² <https://www.who.int/news-room/fact-sheets/detail/ageing-and-health>

²³ Kahn, S. D., & Terry, S. F. [Who owns \(or controls\) health data?](#) Scientific Data, 11(1), 156 (2024).

²⁴ Kiddle, S. J. et al., [Candidate blood proteome markers of Alzheimer's disease onset and progression: a systematic review and replication study](#) Journal of Alzheimer's Disease, 38(3), 515-531 (2014).

²⁵ Jack Jr, C. R. et al., [NIA-AA research framework: toward a biological definition of Alzheimer's disease](#) Alzheimer's & Dementia, 14(4), 535-562 (2018).

²⁶ Dubois, B. et al., [Biomarkers in Alzheimer's disease: role in early and differential diagnosis and recognition of atypical variants](#) Alzheimer's Research & Therapy, 15(1), 175 (2023).

²⁷ Teunissen, C. E. et al., [Blood-based biomarkers for Alzheimer's disease: towards clinical implementation](#) The Lancet Neurology, 21(1), 66-77 (2022).

1.3 The 2D-BioPAD Framework

2D-BioPAD aims to deliver a paper-based platform based on the use of aptamers as recognition element, graphene-based material as a transducer, magnetic nanoparticles for sample purification, flow control, and signal amplification, for the detection of AD biomarkers (**Figure 3**). The 2D-BioPAD platform consists of a paper-based substrate with a sampling pad, detection zone and absorbent pad (A1) and (B1); a passivation layer and an array of graphene functionalised electrodes with single strand DNA (A2), or an array of graphene field effect transistors (B2). These components are contained in a disposable cassette with the corresponding connections for the electrodes, presenting the 2D-BioPAD device (3). The 2D-BioPAD cassette/device is then connected to an external device to induce and control the magnetic field along the strip, and a potentiostat for the electrochemical measurements (4); and finally, a smartphone with a dedicated app for controlling the device and extracting the measurements, offering also the needed visualisation for the end-user (5).

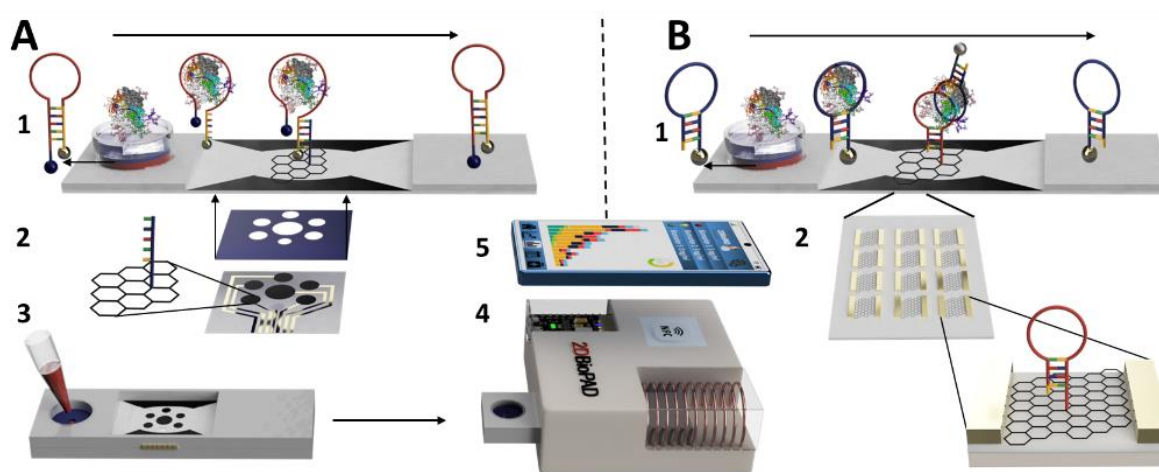


Figure 3: 2D-BioPAD system concept.

Paper-based lateral-flow biosensor assays (LFA) have become a valuable and popular tool for PoC IVD,^{28,29} serving as an alternative to PCR.³⁰ These biosensors are easy to use, portable, provide real-time analysis in a single step, and are inexpensive to manufacture with a good shelf life.³¹ However, they have limitations such as low sensitivity, binary results (positive/negative), difficulty handling complex matrices like blood or serum, and a limited number of detectable biomarkers simultaneously, which restrict their use for conditions like AD. Electrochemical paper-based analytical devices (ePADs), offer sensitive, portable, disposable, and cost-effective solutions by generating an electrochemical signal directly related to the analyte amount. Electrochemical biosensors work by converting a biochemical signal into an electrical signal (current, potential, conductance, or impedance) through a redox reaction, which is then measured by the transducer to quantify the result. These advancements make ePADs a promising alternative for more complex and sensitive diagnostic applications.³²

²⁸ Parolo, C. et al., [Tutorial: design and fabrication of nanoparticle-based lateral-flow immunoassays](#) Nature Protocols 15(12), 3788-3816 (2020).

²⁹ Sena-Torralba, A. et al. [Toward Next Generation Lateral Flow Assays: Integration of Nanomaterials](#) Chemical Reviews, 122(18): 14881–14910 (2022).

³⁰ Merkoçi, A. et al. [COVID-19 biosensing technologies](#) Biosensors and Bioelectronics, 178: 113046 (2021).

³¹ Miku, E. [Recent advancements in electrochemical biosensors for Alzheimer's disease biomarkers detection](#). Current Medicinal Chemistry, 28(20), 4049-4073 (2021).

³² Solhi, E. et al., [Electrochemical paper-based analytical devices \(ePADs\) toward biosensing: recent advances and challenges in bioanalysis](#). Analytical methods, 12(11), 1398-1414 (2020).

Research has focused on improving ePAD functionality, especially electrode technology, to enhance electrical signals and simplify functionalization.³³

The 2D-BioPAD project aims to create a non-invasive, cost-effective tool for early AD diagnosis, with the goal of improving the treatment outcomes and reducing burdens. This project addresses the current challenges such as lengthy diagnostic timelines and inadequate biomarker diagnostics. In developing effective diagnostic tools for AD, it is crucial to differentiate between functional and non-functional technical specifications. Making this distinction ensures a comprehensive understanding of the system's requirements and supports the successful design and implementation of innovative diagnostic solutions.

By addressing these functional and non-functional specifications, the 2D-BioPAD project aims to develop a robust, user-centric diagnostic aid that enhances early detection and monitoring of Alzheimer's Disease, ultimately improving patient outcomes and reducing the burden on healthcare systems.

1.4 Biomarkers Binding: The role of Aptamers and Nanoparticles

Aptamers are short DNA or RNA sequences that mimic antibodies, known for their high specificity and affinity. They are cheaper, easier to produce, more stable, and non-toxic compared to antibodies, making them ideal for bio-analysis and therapeutics.³⁴ Aptamers can target various analytes and have been integrated into nanomaterials, enhancing their performance and commercial potential in low-cost diagnostic systems.³⁵ They offer a validated alternative to antibodies for diagnostic and analytical applications, including the quantitative detection of Alzheimer biomarkers.^{36,37} Compared to antibodies, aptamers provide a lower LOD, higher stability, lower cost and more flexible design while also being capable of distinguishing between different isoforms of the same protein.^{38,39}

Identified using SELEX, aptamers face challenges like lengthy development times and low success rates,^{40,41} but advancements in selection methods are improving outcomes.^{42,43} Since the first aptamers targeting A β peptides were reported in 2002,⁴⁴ many studies have used them to target AD biomarkers.⁴⁵ Electrochemical aptasensors, in particular, have shown promise in detecting AD biomarkers such as A β 40, A β 42, and tau protein isoforms like p-Tau231, often outperforming

³³ Bhattacharya, G. et al., [Disposable paper-based biosensors: Optimizing the electrochemical properties of laser-induced graphene](#) ACS Applied Materials & Interfaces, 14(27), 31109-31120 (2022).

³⁴ Shui, B. et al., [Biosensors for Alzheimer's disease biomarker detection: a review](#) Biochimie, 147, 13-24 (2018).

³⁵ Kim, Y. S. Et al., [Aptamer-based nanobiosensors](#) Biosensors and Bioelectronics, 76, 2-19 (2016).

³⁶ Scarano, S. et al. [Detecting Alzheimer's disease biomarkers: From antibodies to new bio-mimetic receptors and their application to established and emerging bioanalytical platforms e A critical review](#) Analytica Chimica Acta 940 21e37 (2016).

³⁷ Zamanian, J. et al. [Current progress in aptamer-based sensing tools for ultra-low level monitoring of Alzheimer's disease biomarkers](#) Biosensors and Bioelectronics 197, 113789 (2022).

³⁸ Mikuła E. [Recent Advancements in Electrochemical Biosensors for Alzheimer's Disease Biomarkers Detection](#) Current medicinal chemistry, 28(20), 4049–4073 (2021).

³⁹ Zheng, Y., et al. [Advances in aptamers against A \$\beta\$ and applications in A \$\beta\$ detection and regulation for Alzheimer's disease](#) Theranostics, 12(5), 2095–2114 (2022).

⁴⁰ Tuerk, C., & Gold, L. [Systematic evolution of ligands by exponential enrichment: RNA ligands to bacteriophage T4 DNA polymerase](#) Science, 249(4968), 505-510 (1990).

⁴¹ Ellington, A. D., & Szostak, J. W., [In vitro selection of RNA molecules that bind specific ligands](#) Nature, 346(6287), 818-822 (1990).

⁴² Chen, Z. et al., [Artificial intelligence in aptamer–target binding prediction](#) International journal of molecular sciences, 22(7), 3605 (2021).

⁴³ Mikuła, E., & Malecka-Baturo, K. [An Overview of the Latest Developments in the Electrochemical Aptasensing of Neurodegenerative Diseases](#) Coatings, 13(2), 235 (2023).

⁴⁴ Ylera, F., et al., [Selection of RNA aptamers to the Alzheimer's disease amyloid peptide](#) Biochemical and biophysical research communications, 290(5), 1583-1588 (2002).

⁴⁵ Murakami, K. et al., [Aptamers targeting amyloidogenic proteins and their emerging role in neurodegenerative diseases](#) Journal of Biological Chemistry, 298(1) (2022).

traditional ELISA methods.^{46, 47, 48, 49} However, creating aptasensors that can simultaneously detect multiple biomarkers remains a challenge.

Among nanomaterials, MNPs are extensively utilized in life sciences due to their high surface-to-volume ratio, superparamagnetic nature, excellent biocompatibility, low toxicity, and site-specific targeting ability. They are cost-effective and sustainable to manufacture, enhancing their appeal for various biomedical applications.⁵⁰ When integrated with biosensors, MNPs significantly improve sensitivity and reliability.⁵¹ They play a crucial role in sample purification, minimizing non-specific signals, and regulating flow during various stages of bioassays, such as bioreceptor incubation, purification, recognition, and signal acquisition.^{52,53} Magnetically responsive nanoparticles can target and interact with specific proteins through appropriate surface functionalization or conjugation with probes like antibodies or aptamers. They can be precisely controlled by an external magnetic field, facilitating the quantification of bound targets by supporting fine-tuned separation or magnetic signal readout, with minimal interference with biological samples.⁵⁴ Various nanoparticles, including gold and silver NPs, quantum dots, graphene oxide NPs, Prussian Blue NPs, carbon nanostructures, and various forms of MNPs, have been employed in biosensing techniques for AD.^{55,56}

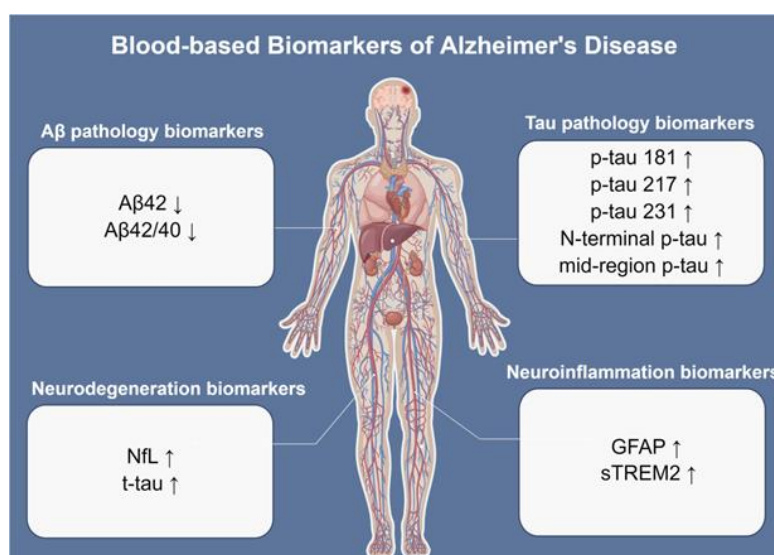


Figure 4: Overview of 2D-BioPAD AD biomarkers⁵⁷.

These nanomaterials have been used to detect blood biomarkers like Aβ40, Aβ42, and p-Tau with good selectivity, specificity, fast response, and low limits of detection (LOD), across different stages of AD.^{58,59}

- ⁴⁶ Khang, A. et al., [A cost-effective aptasensor capable of early diagnosis and monitoring of Alzheimer's disease with the rapid analysis of beta-amyloid peptide 1–40](#) *Sensors & Diagnostics*, 2(2), 409-417 (2023).
- ⁴⁷ Negahdary, M. et al., [Aptasensing of beta-amyloid \(Aβ \(1–42\)\) by a 3D-printed platform integrated with leaf-shaped gold nanodendrites](#) *Sensors and Actuators B: Chemical*, 393, 134130 (2023).
- ⁴⁸ Jia, Z. et al., [CRISPR-Powered Aptasensor for Diagnostics of Alzheimer's Disease](#) *ACS sensors*, 9(1), 398-405 (2023).
- ⁴⁹ Phan, L. M. T., & Cho, S. [Fluorescent aptasensor and colorimetric aptablot for p-Tau231 detection: Toward early diagnosis of Alzheimer's disease](#) *Biomedicines*, 10(1), 93 (2022).
- ⁵⁰ Chavan, N. et al., [Magnetic nanoparticles—A new era in nanotechnology](#) *Journal of Drug Delivery Science and Technology*, 77, 103899 (2022).
- ⁵¹ Le, T. D. et al., [State of the art on the separation and purification of proteins by magnetic nanoparticles](#) *Journal of Nanobiotechnology*, 21(1), 363 (2023).
- ⁵² Esmaili, E. et al., [Hybrid Magnetic-DNA Directed Immobilisation Approach for Efficient Protein Capture and Detection on Microfluidic Platforms](#) *Scientific reports*, 7(1), 194 (2017).
- ⁵³ Zhu, N. et al., [DNA Hybridization at Magnetic Nanoparticles with Electrochemical Stripping Detection](#) *Electroanalysis*, 16(23), 1925-1930 (2004).
- ⁵⁴ Cao, B. et al., [Development of magnetic sensor technologies for point-of-care testing: Fundamentals, methodologies and applications](#) *Sensors and Actuators A: Physical*, 312, 112130 (2020).
- ⁵⁵ Hou, F. et al., [The application of nanoparticles in point-of-care testing \(POCT\) immunoassays](#) *Analytical Methods* 15, 2154-2180 (2023).
- ⁵⁶ Xianyu, Y. et al., [Magnetic particles-enabled biosensors for point-of-care testing](#) *Trends Analytical Chemistry*, 106, 213-224 (2018).
- ⁵⁷ Tao, Q. Q., Lin, R. R., & Wu, Z. Y. [Early Diagnosis of Alzheimer's Disease: Moving Toward a Blood-Based Biomarkers Era](#) *Clinical Interventions in Aging*, 353-358 (2023).
- ⁵⁸ Devi, R. et al., [Au/NiFe₂O₄ nanoparticle-decorated graphene oxide nanosheets for electrochemical immunosensing of amyloid beta peptide](#) *Nanoscale Advances*, 2(1), 239-248 (2020).
- ⁵⁹ Chiu, M. J. et al., [Nanoparticle-based immunomagnetic assay of plasma biomarkers for differentiating dementia and prodromal states of Alzheimer's disease—A cross-validation study](#) *Nanomedicine: Nanotechnology, Biology and Medicine*, 28, 102182 (2020).

A list of 2D-BioPAD AD biomarkers under study is depicted in **Figure 4** with relative descriptions reported below.

Beta amyloid (A β): *Under normal conditions, A β is a soluble product of neuronal metabolism essential for synaptic function.⁶⁰ A β 40 and A β 42 monomers are crucial for synaptic plasticity and neuronal survival. However, under pathological conditions, A β aggregates into oligomers and plaques due to an imbalance between its production and extracellular clearance, particularly A β 42, which is more prone to aggregation and considered toxic. These plaques can disrupt neural networks and communication.⁶¹ When A β accumulates in the brain, its levels decrease in CSF and blood,⁶² making A β a core biomarker for AD.⁶³*

Tau protein (tau): *Tau protein, primarily associated with axonal microtubules, plays a role in signaling within dendrites.⁶⁴ Under pathological conditions, tau becomes hyperphosphorylated and forms neurofibrillary tangles (NFTs), leading to microtubule disintegration, disrupted signaling, and cell death.⁶⁵ Research and commercial assays focus on various phosphorylated forms of tau, including p-Tau181, p-Tau217, and p-Tau231, which are associated with different stages of AD progression. Phosphorylated tau versions in plasma, especially p-Tau217, are good predictors of AD and cognitive decline, with p-Tau217 showing the largest fold-change between AD and non-AD disorders.⁶⁶*

Neurofilament Light and Neurodegeneration: *Neurofilament light (NfL) polypeptide, a component of the neural cytoskeleton, is a well-established marker of neuroaxonal injury and neurodegeneration. Under normal conditions, Plasma NfL correlates well with CSF measures for both MCI and AD,⁶⁷ making it a good blood-based biomarker. However, NfL is not specific to AD, as it also indicates other types of neurodegeneration, including different dementia types such as frontotemporal, vascular, and HIV-associated dementias.⁶⁸*

Neuroinflammation: *Glial fibrillary acidic protein (GFAP) is a well-studied glial marker released in response to A β pathology.⁶⁹ GFAP, found in astrocytes, is released into CSF and blood when these cells are damaged.*

⁶⁰ Parihar, M. S. et al., [Amyloid- \$\beta\$ as a modulator of synaptic plasticity](#) Journal of Alzheimer's Disease, 22(3), 741-763 (2010).

⁶¹ Hampel, H. et al., [The amyloid- \$\beta\$ pathway in Alzheimer's disease](#) Molecular psychiatry, 26(10), 5481-5503 (2021).

⁶² Klafki, H. W. et al., [Is plasma amyloid- \$\beta\$ 1-42/1-40 a better biomarker for AD than A \$\beta\$ X-42/X-40?](#) Fluids and Barriers of the CNS, 19(1), 96 (2022).

⁶³ Pais, M. V. et al., [Plasma biomarkers of Alzheimer's disease: a review of available assays, recent developments, and implications for clinical practice](#) Journal of Alzheimer's Disease Reports, (Preprint), 1-26 (2023).

⁶⁴ Grundke-Iqbal, I. et al., [Abnormal phosphorylation of the microtubule-associated protein tau \(tau\) in Alzheimer cytoskeletal pathology](#) Proceedings of the National Academy of Sciences, 83(13), 4913-4917 (1986).

⁶⁵ Mietelska-Porowska, A. et al., [Tau protein modifications and interactions: their role in function and dysfunction](#) International journal of molecular sciences, 15(3), 4671-4713. (2014).

⁶⁶ Ashton, N. J. et al., [Plasma and CSF biomarkers in a memory clinic: head-to-head comparison of phosphorylated tau immunoassays](#) Alzheimer's & Dementia, 19(5), 1913-1924 (2023).

⁶⁷ Gaetani, L. et al., [NfL chain as a biomarker in neurological disorders](#). Journal of Neurology, Neurosurgery & Psychiatry, 90(8), 870-881 (2019).

⁶⁸ Bridel, C. et al., [Diagnostic value of cerebrospinal fluid neurofilament light protein in neurology: a systematic review and meta-analysis](#). JAMA neurology, 76(9), 1035-1048 (2019).

⁶⁹ Morgan, A. R. et al., [Inflammatory biomarkers in Alzheimer's disease plasma](#). Alzheimer's & dementia, 15(6), 776-787 (2019).

1.5 Biomarkers Binding: Quantitative Analysis

AD is strongly associated with inflammatory dysregulation,⁷⁰ which may be attributed to disruptions in commensal microbiota, chronic microbial infections,⁷¹ chronic astrogliosis,⁷² and microglial exacerbation,⁷³ often triggered by pathological aggregates of amyloid beta-42 peptide (A β 42) and hyperphosphorylated tau protein (p-tau). However, the exact contribution of inflammation to the disease progression remains incompletely understood.⁷⁴ The levels of various cytokines are considered indicators of neuroinflammation, potentially increasing as the disease progresses or temporarily from the MCI stage to AD.⁷⁵ Given that many therapies for AD have proven inadequate or ineffective, early diagnosis may hold the key to managing the disease effectively. Accurate diagnosis and effective treatment are considered pivotal in the medical field, driving significant research into developing next-generation materials for successful diagnosis and therapy.⁷⁶

Sensitivity is a critical parameter for biosensors, including apta-sensors, which is addressed in the 2D-BioPAD project. This project integrates aptamers targeting 5 different biomarkers into an innovative biochip for a multiplexed assay.

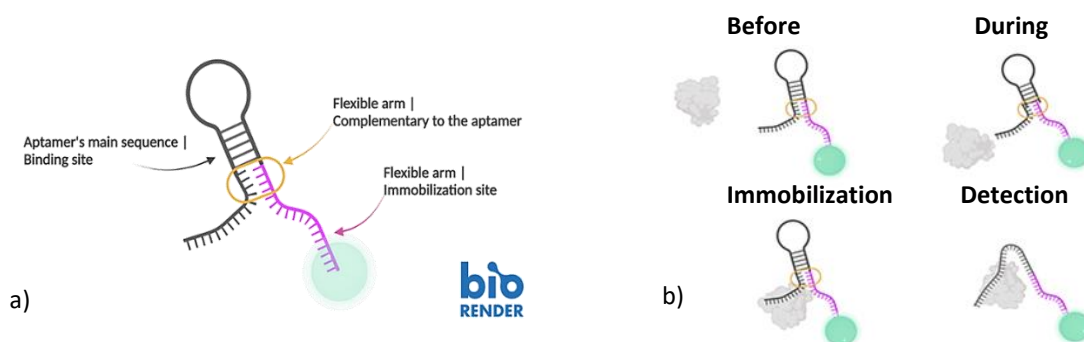


Figure 5: a) Schematic illustration of an MNP conjugated with an aptamer b) Illustration of the optimum scenario, one 1 MNP \leftrightarrow 1 aptamer \leftrightarrow 1 biomarker including 4 steps: Before conjugation, During conjugation, Immobilization and detection

The integration of biomolecules and nanomaterials has revolutionized the diagnosis and treatment of various diseases, including cancers. Biocompatible molecules such as DNA, RNA, and peptides enable precise targeting and imaging, while the unique spectroscopic and thermotherapeutic properties of nanomaterials offer significant advantages in sensing, imaging, and therapeutic applications.⁷⁷ Nanoparticles serve as effective scaffolds for assembling nanoparticle-based biosensors.⁷⁸ Gold nanoparticles, in particular, are well-suited for bioconjugation due to their compatibility and ability to readily bind with various biomolecules such as amino acids, proteins, enzymes, and DNA.⁷⁹

⁷⁰ Faria, M.C. et al., [Increased plasma levels of BDNF and inflammatory markers in Alzheimer's disease](#) J. Psychiatr. Res. Journal of Psychiatric Research, 53 166-172 (2014).

⁷¹ Ashraf, G.M. et al., [The Possibility of an Infectious Etiology of Alzheimer Disease](#) Mol. Neurobiol. 56, 4479–4491 (2014).

⁷² Katsipis, G. et al., [Salivary GFAP as a potential biomarker for diagnosis of mild cognitive impairment and Alzheimer's disease and its correlation with neuroinflammation and apoptosis](#) J. Neuroimmunol. 361, 577744 (2021).

⁷³ Heneka, M.T. et al., [Innate immunity in Alzheimer's disease](#) Nature Immunology volume 16, pages229–236 (2015).

⁷⁴ Calsolaro, V., Edison, P., [Neuroinflammation in Alzheimer's disease: Current evidence and future directions](#) Alzheimer's Dement. 12, 6, 719-732 (2016).

⁷⁵ Brosseron, F. et al., [Body Fluid Cytokine Levels in Mild Cognitive Impairment and Alzheimer's Disease: a Comparative Overview](#) Mol. Neurobiol. 50, 534–544, (2014).

⁷⁶ Carothers, J.M. et al., [Aptamers selected for higher-affinity binding are not more specific for the target ligand](#) J. Am. Chem. Soc. 128, 24, 7929–7937 (2006).

⁷⁷ Jo, H., Ban, C., [Aptamer-nanoparticle complexes as powerful diagnostic and therapeutic tools](#) Exp. Mol. Med. 48, e230 (2016).

⁷⁸ Niemeyer, C.M., [Nanoparticles, proteins, and nucleic acids: Biotechnology meets materials science](#) Angew. Chemie - Int. Ed. 40, 22, 4128-4158 (2001).

⁷⁹ Zheng, J. et al., [An aptamer-based assay for thrombin via structure switch based on gold nanoparticles and magnetic nanoparticles](#) Talanta 80,5, 1868–1872 (2010).

Additionally, magnetic nanoparticles are widely utilized in bioanalysis and pharmaceutical detection due to their unique magnetic properties.⁸⁰

The approach followed in WP2 is crucial not only for preserving the sophisticated tertiary structure of the aptamers, and thus their binding affinity, but also for maintaining the MNPs features.⁸¹ Typically, aptamer tertiary structures are very robust; unless chemically modified (e.g., under highly acidic pH conditions), aptamers will refold into their «native» structure once environmental conditions are restored. As illustrated in **Figure 5**, the short and flexible arm of deoxyribonucleotides is vital for the interaction between the MNP and the aptamer's secondary structure. This flexibility allows for the efficient replacement of the aptamer if new biomarkers emerge. Optimized aptamers are then end-functionalized with appropriate groups for immobilization such as a carbon linker between the amino group and the oligonucleotide's end. Aptamers' size, solution ionic strength, thermodynamic effects, and DNA structure all influence MNPs' coverage and aptamers' arrangement.⁸² Well-established cross-linking methodologies for immobilizing DNA sequences on MNPs are examined and evaluated.⁸³ Additionally, AI methods, such as sequence clustering on SELEX pools, can evaluate aptamer similarities,⁸⁴ while Graph Transformers analyse their structure to predict binding affinity.⁸⁵

MNPs are exploited to facilitate sample purification, minimize non-specific signals, and act as flow control at various stages of the bioassay, including bioreceptor incubation, purification, recognition, and signal acquisition.^{86,87} In the first stage, the flow and position of MNPs are magnetically controlled, ensuring proper orientation and reducing the number of aptamers conjugated to the MNPs. This precise control of MNPs and the magnetic field is expected to achieve a 1:1 aptamer-to-MNP ratio (**Figure 5**). Then, the MNP/aptamer conjugates will be regionally retained while in 2nd stage the magnetic field is directed towards the electrodes where the recognition process occurs. Finally, in 3rd stage, MNPs not binding to the electrode are eliminated towards an absorbent pad. At each specific stage, magnetic field parameters (such as field amplitude, duration, field sign) will be independently optimized to maximize the signal acquisition).

⁸⁰ Wang, J., Kawde, A.N., [Magnetic-field stimulated DNA oxidation](#) Electrochem. commun. 4, 4, 349-352 (2002).

⁸¹ Haddad, Y., et al., [The Isolation of DNA by Polycharged Magnetic Particles: An Analysis of the Interaction by Zeta Potential and Particle Size](#) International journal of molecular sciences, 17(4), 550 (2016).

⁸² Song, J., et al., [Based on DNA Strand Displacement and Functionalized Magnetic Nanoparticles: A Promising Strategy for Enzyme Immobilization](#). Ind. Eng. Chem. Res., 56(17), 5127–5137 (2017).

⁸³ Clinton, Y., Lan H., [New advances in cross-linking mass spectrometry toward structural systems biology](#) Current Opinion in Chemical Biology, 76, 102357 (2023).

⁸⁴ Bashir, A. et al., [Machine learning guided aptamer refinement and discovery](#) Nature Communications volume 12, 2366 (2019).

⁸⁵ Wornow, M. [Applying Deep Learning to Discover Highly Functionalized Nucleic Acid Polymers That Bind to Small Molecules](#) Bachelor's thesis, Harvard College (2020).

⁸⁶ Esmaeili, E., et al., [Hybrid Magnetic-DNA Directed Immobilisation Approach for Efficient Protein Capture and Detection on Microfluidic Platforms](#) Sci. reports, 7(1), 194 (2017).

⁸⁷ Zhu, N., et al., [DNA Hybridization at Magnetic Nanoparticles with Electrochemical Stripping Detection](#) Electroanalysis, 16(23), 1925-1930 (2004).

2. Conjugation Design, Synthesis, and Selection

WP2 named Biomarkers binding and quantitative analysis includes 4 tasks, and 4 deliverables outlined in **Figure 6**. Currently Tasks 2.1 and 2.3 are underway while Tasks 2.2 and 2.4 are in preparatory phases.

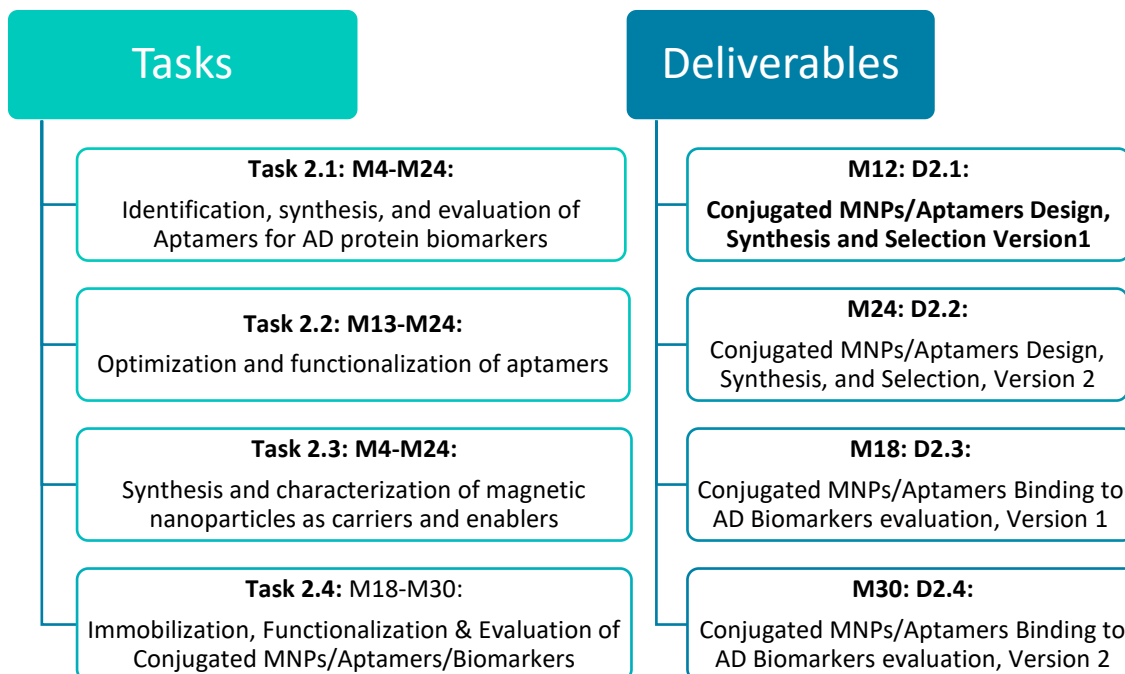


Figure 6: Schematic outline of Work Package 2: Biomarkers binding and quantitative analysis.

What follows is a brief progress per task for WP2:

Task 2.1: Identification, Synthesis, and Evaluation of Aptamers for AD Protein Biomarkers

This task begins with the identification of aptamers specific to AD protein biomarkers, such as A β ₁₋₄₀, A β ₁₋₄₂, tau₁₈₁, tau₂₁₇, tau₂₃₁, NFL and GFAP. The process involves an extensive literature review and database search to collect all available DNA aptamer sequences that have been previously reported for these targets. Following this, a comparative study will be conducted to evaluate the characteristics, binding properties, and evaluation techniques of the aptamers suggested. Eventually, up to five DNA aptamers per target, with the most robust properties, are currently evaluated for their binding affinity (k_{on} , k_{off} , K_d) using techniques like Surface Plasmon Resonance (SPR) or BioLayer Interferometry (BLI) under appropriate buffer conditions. The specificity of these aptamers is also being assessed to avoid non-specific binding to unintended protein targets, which could reduce assay specificity. For AD biomarkers that lack aptamer sequences in the literature, in vitro selection of DNA aptamers will be performed using the Novaptech SELEX procedure. Proprietary random oligonucleotide libraries will be used. A diversity of 10^{14} - 10^{15} will be experimentally explored by iterative selection/amplification steps. This exploration process will become incrementally guided as the selected aptamers will feed deep learning models capable of predicting structures of high affinity, easing the process after each iteration. The evolution of the pools is monitored by NGS sequencing, and the sequence analyses with a proprietary algorithm. Candidates chosen based on the bioinformatics analysis will be chemically synthesized and their binding to proteins will be characterized by SPR or BLI.

Task 2.2: Optimization and functionalization of aptamers

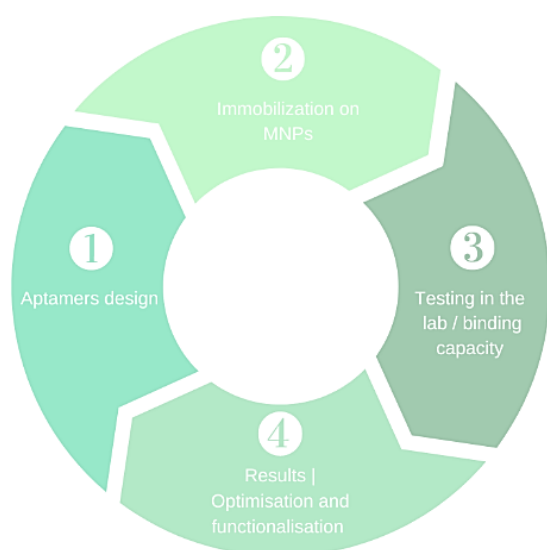
DNA aptamer length affects its immobilization and cost. Specifically, the longer the aptamer, the lower the immobilization effectiveness might be. Consequently, in this task the size of aptamers will be evaluated and optimized. Truncated variants of aptamers will be designed based on their predicted secondary structure, chemically synthesized, and studied with respect to their binding properties (SPR or BLI). Aptamers corresponding to the minimal oligonucleotide displaying the properties of the parent aptamer will be further elaborated while one of the 2 fixed flanks of the full-length aptamer may serve for immobilization purposes on MNPs. Such modified aptamers will be evaluated by either SPR or BLI protocol. These binding properties will be used as features to, along with the structure, train a deep learning model aiding length optimization.

Task 2.3: Synthesis and Characterization of Magnetic Nanoparticles as Carriers and Enablers

This task focuses on the synthesis and characterization of MNPs to be utilized as carriers and enablers in bioassays, facilitating sample purification, minimizing non-specific signals, and controlling flow during various stages, such as bioreceptor incubation, purification, recognition, and signal acquisition. Magnetite (Fe_3O_4) MNPs have been synthesized with a focus on producing nanoparticles of varying sizes and are currently rigorously characterized structurally, morphologically, and magnetically (TEM, XRD, VSM) since the size of the MNPs is directly reflected to their magnetic response and in turn their interaction with external magnetic fields while may affect specifically and selectively the aptamer immobilization to be held in T2.4. MNPs with diameters ranging from 10 nm up to 250 nm have been used for the immobilization of DNA aptamers for a variety of applications. Generally, the smaller the size of MNPs, the fewer the number of aptamers immobilized together with more homogeneous distributions of immobilized aptamers, concluding on enhanced analytical performance of the assay. To provide electrochemical sensing via electrical conductivity biphasic MNPs are manufactured composed of a gold contact and a magnetic part in variable designations. These hybrid MNPs will be conjugated with DNA aptamers following established protocols. After conjugation, the MNP-aptamer complexes will be purified to remove any unbound aptamers or by-products, ensuring that the final MNPs are ready for integration into the bioassay platform.

Task 2.4: Immobilization | Functionalization | Evaluation of Conjugated MNPs/Aptamers/Biomarkers

Well established cross-linking methodologies for DNA sequences immobilization on MNPs are currently examined and evaluated. Following, a systematic investigation of the binding capacity of



conjugated MNPs/Aptamers with the selected biomarkers in simple and complex solutions (artificial CSF and plasma) will be performed. Concentrations of amyloid beta are around 10-fold lower in plasma than in CSF, whereas the total protein content in the plasma is 10-fold higher. This renders the detection of the selected biomarkers difficult, and a higher specificity and sensitivity might be needed.

Following a 4-step iterative process, WP2 *Biomarkers binding and quantitative analysis* initiated with an extended literature review and search in databases for all the available sequences of DNA aptamers for the selected biomarkers,

towards selecting the most appropriate primary structure, and designing the secondary structure according to the sensing strategies (Step 1). Currently, the required aptamers are sought by NovapTech SELEX procedure, employing proprietary random oligonucleotide libraries and AI techniques (CeADAR, UCD). What follows is aptamer characterization, and individual design optimization (size, buffer, ionic strength, pH, etc.), with emphasis on selectivity and sensitivity. In parallel, MNPs have been synthesized and characterized. These MNPs are critical for facilitating sample purification, reducing non-specific signals, and controlling the flow of materials at various stages of the bioassay, where required. The integration of MNPs ensures that the aptamers remain oriented and functional throughout the bioassay process, enhancing the overall reliability and accuracy of biomarker detection.

Step 2 involves the immobilization of the aptamers on the MNPs. An analysis of the kinetic model of immobilization should be made with respect to the size of the MNP and the size of the aptamer. The immobilization technique is based on well-established cross-linking methodologies, aiming to (i) provide an adaptable and scalable solution that can easily evolve in case other biomarkers are identified and requested; and (ii) target a 1 (MNP): 1 (Aptamer) ratio to be achieved, further increasing the selectivity and specificity capability per biomarker.

The conjugated MNPs/Aptamers will be tested at lab environment with all biomarkers to evaluate their binding capacity (Step 3).

Finally, possible redesign and optimization might be needed after the first testing (Step 4). Immobilization on MNPs might change the binding capacity and specificity of the aptamers. Thus, it is essential to use our results as input for optimization of the final product before the involvement of graphene.

2.1 Aptamers' Identification

In Task 2.1 of the WP2, CeADAR focused on the identification of aptamers and evaluation of their binding affinity to AD protein biomarkers. As a part of this effort, CeADAR conducted a literature search to identify, compare, and assess advanced computational methodologies used in aptamer binding research, including MLPD⁸⁸, RaptGen⁸⁹, Aptanet⁹⁰, APIPred⁹¹, AptabERT⁹², Aptatrans⁹³, and AptamCTS (Monte-Carlo Tree Search)⁹⁴ as outlined in **Table 2**.

These methodologies span a broad spectrum of techniques, from experimental approaches enhanced by machine learning to state-of-the-art transformer-based models designed for predicting and generating high-affinity aptamer sequences. Each method was meticulously evaluated based on its core description, key features, and inherent limitations, which subsequently informed their functionality ratings and suitability for specific research contexts.

For example, **MLPD (2021)** is distinguished by its integration of fully connected and convolutional neural network models to predict aptamer affinities directly from sequence data.⁹⁰ This method synergizes Particle Display for experimental affinity partitioning with in silico predictions, achieving an

⁸⁸ Bashir, A. et al., [Machine learning guided aptamer refinement and discovery](#) *Nat Commun* 12, 2366 (2021).

⁸⁹ Iwano, N. et al., [Generative aptamer discovery using RaptGen](#) *Nat Comput Sci* 2, 378–386 (2022).

⁹⁰ Emami, N. et al., [Aptanet as a deep learning approach for aptamer–protein interaction prediction](#) *Sci Rep* 11, 6074 (2021).

⁹¹ Fang, Z. et al., [APIPred: An XGBoost-Based method for predicting aptamer–protein interactions](#) *J. Chem. Inf. Model.* 64, 7 (2023).

⁹² Morsch, F. et al., [AptabERT: Predicting aptamer binding interactions](#) *bioRxiv*, 2023-11 (2023).

⁹³ Shin, I. et al., [Aptatrans: a deep neural network for predicting aptamer-protein interaction using pretrained encoders](#) *BMC Bioinformatics* 24, 447 (2023).

⁹⁴ Lee, G. et al. [Predicting aptamer sequences that interact with target proteins using an aptamer–protein interaction classifier and a Monte Carlo tree search approach](#). *PLOS ONE*, 16(6), e0253760 (2021).

11-fold improvement over random selection methods. Notably, MLPD has been successful in generating aptamers with superior binding affinity, including the design of truncated sequences that, despite their reduced length, exhibit enhanced binding affinity (1.5 nM). However, its effectiveness is heavily dependent on the availability of extensive, high-quality experimental data to train its machine learning models.

Similarly, **RaptGen (2022)** employs a variational autoencoder for in silico aptamer generation, leveraging a profile Hidden Markov Model decoder for robust motif sequence representation.⁹¹ RaptGen excels in embedding simulation sequence data into a low-dimensional latent space, facilitating the generation of novel aptamers not captured in high-throughput sequencing data. Despite its innovative approach, RaptGen faces challenges related to the computational cost of profile HMM sequence probability calculations, which results in longer training times and necessitates further optimization for improved efficiency.

AptaNet (2021), a deep neural network model, focuses on predicting aptamer-protein interactions (API) with greater accuracy than traditional MLP and CNN approaches.⁹² By utilizing a Random Forest strategy to identify 193 optimal features, AptaNet enhances the precision and relevance of its predictions. However, it struggles with the limitations posed by scarce and imbalanced datasets, which can constrain its training and predictive capabilities.

APIPred (2023) introduces an XGBoost-based model designed for high-accuracy API predictions, combining k-mer frequency with reverse complement k-mer frequency analysis.⁹³ APIPred achieves a leading accuracy of 96.5% on its development dataset, validated through molecular docking, MD simulations, and SPR binding assays. Nonetheless, the model's robustness is limited by the relatively small dataset size, underscoring the need for larger, more diversified datasets.

AptaBERT (2023), utilizing a BERT-based architecture, is trained on an extensive dataset to predict aptamer-target interactions.⁹⁴ It employs a two-step process, beginning with the pre-training of an unsupervised Masked Language Model followed by fine-tuning with supervised classification on labeled data. AptaBERT achieves remarkable performance with a ROC-AUC of 96% for protein targets and 85% for small molecule interactions, outpacing benchmark models by significant margins. However, its applicability is limited by the high computational resources required for training and fine-tuning, posing a barrier for researchers with limited access to such resources.

AptaTrans (2023) integrates pretrained encoders for API prediction, utilizing advanced tokenization and transformer-based encoders, combined with convolutional blocks and fully connected layers.⁹⁵ AptaTrans implements self-supervised learning for masked token and secondary structure prediction, which significantly enhances the model's accuracy and generalization capabilities. The model's performance, reflected in a ROC-AUC score that surpasses other leading models, is nonetheless challenged by the scarcity of high-quality, annotated datasets for aptamer-protein interactions.

Lastly, **Apta-MCTS (2021)** combines a Monte-Carlo Tree Search (MCTS) algorithm with a Random Forest-based API classifier to generate RNA aptamer sequences targeting specific proteins.⁹⁴ While DNA aptamers are widely used in molecular binding studies, the decision to focus on RNA aptamers is motivated by factors that provide significant advantages in this particular application. First, RNA aptamers are known for their structural flexibility, which is due to the additional hydroxyl group at the 2' position of the ribose sugar. This enables them to form more complex three-dimensional structures

that are essential for high-affinity binding to protein targets.^{95,96} According to Lee et al.⁹⁷, RNA aptamers generated using the Apta-MCTS model achieved higher binding affinity compared to DNA aptamers in similar settings. The study demonstrated that the iterative nature of the MCTS algorithm, combined with Random Forest classification, allowed RNA aptamers to be tailored more effectively for target proteins like beta-amyloid peptide (1-42), crucial in Alzheimer's Disease (AD) biomarker detection.

Moreover, RNA aptamers are typically better suited for targeting complex or challenging proteins, as they are capable of adopting a wider range of secondary and tertiary structures. Unlike traditional methods, the Apta-MCTS model was designed to exploit this variability, generating aptamers of different lengths and testing them for binding efficiency. This adaptability is particularly important when targeting proteins such as beta-amyloid peptide (1-42) in AD, which involves highly specific binding regions. Validated via ZDOCK docking simulations, Research by Li et al. (2014)⁹⁸ and Lee and Han (2019)⁹⁹ has shown that RNA aptamers generally outperform DNA aptamers in such cases due to their enhanced ability to engage with difficult protein surfaces. While further refinement of the API classifier could enhance its performance, Apta-MCTS offers a flexible approach to aptamer design, reducing reliance on costly and time-consuming experimental methods.

Table 2: Evaluation of Functionalities, Limitations, and Suitability of Computational Aptamer Binding Research Methodologies including MLPD, RaptGen, AptaNet, APIPred, AptaBERT, AptaTrans, and Apta-MCTS.

Methodology	Functionalities	Limitations Rating	Suitability
MLPD, 2021	+++ ++		<i>Seeking a direct bridge between experimental techniques and computational refinement.</i>
RaptGen, 2022	+++ +		<i>Ideal for exploring novel sequences through generative methods, with a focus on motif representation.</i>
AptaNet, 2021	++ ++		<i>Appropriate for those focusing on predicting interactions without the need to generate novel sequences.</i>
APIPred, 2023	+ ++		<i>Suitable for targeted prediction tasks, though details are less clear compared to others.</i>
AptaBERT, 2023	+++ +		<i>Highly effective for understanding complex interactions and discovering new targets, requires substantial data.</i>
AptaTrans, 2023	+++ ++		<i>Optimized for transforming experimental data into high-affinity candidates, particularly efficient in enhancing the selection process through its unique model-guided mutation strategy.</i>
Apta-MCTS, 2021	+++ ++		<i>Suited for generating aptamer sequences with high affinity for specific targets, especially when computational efficiency and iterative optimization are required.</i>

Notation:

Functionalities are rated as "+", "++", or "+++", with "+++" indicating a high level of functionality.

Limitations Rating follows a similar scale, where "+" indicates fewer limitations.

Suitability provides a context for which scenario each methodology might be most appropriate.

⁹⁵ Chushak Y, Stone MO. [In silico selection of RNA aptamers](#). Nucleic Acids Research. 37(12):e87–e87. PMID:19465396 (2009).

⁹⁶ Ahirwar R, et al. [In silico selection of an aptamer to estrogen receptor alpha using computational docking employing estrogen response elements as aptamer-like molecules](#). Scientific reports. 2016;6:21285. PMID:26899418

⁹⁷ Lee, G. et al. [Predicting aptamer sequences that interact with target proteins using an aptamer-protein interaction classifier and a Monte Carlo tree search approach](#). PLOS ONE, 16(6), e0253760 (2021).

⁹⁸ Li BQ, Zhang YC, Huang GH, Cui WR, Zhang N, Cai YD. [Prediction of aptamer-target interacting pairs with pseudo-amino acid composition](#). PLoS One. 2014;9(1). PMID:24466214

⁹⁹ Lee, W., & Han, K. [Constructive prediction of potential RNA aptamers for a protein target IEEE/ACM transactions on computational biology and bioinformatics](#), 17(5), 1476-1482 (2019).

This comprehensive analysis was aimed at refining the selection process and fostering the development of high-affinity aptamer candidates for targeting AD biomarkers.

Additionally, we thoroughly checked existing databases such as Apta-Index, Aptagen¹⁰⁰ and the UTexas¹⁰¹ database to support our research efforts. Following the guideline outlined by Lee et al., 2021⁹⁶, as depicted in **Figure 7**, we performed a Apta-MCTS model protocol. CeADAR focused on proposing candidate aptamers by targeting the beta-amyloid peptide (1-42) sequence, “DAEFRHDSGYEVHHQKLVFFAEDVGSNKGAIIGLMVGGVVIA”

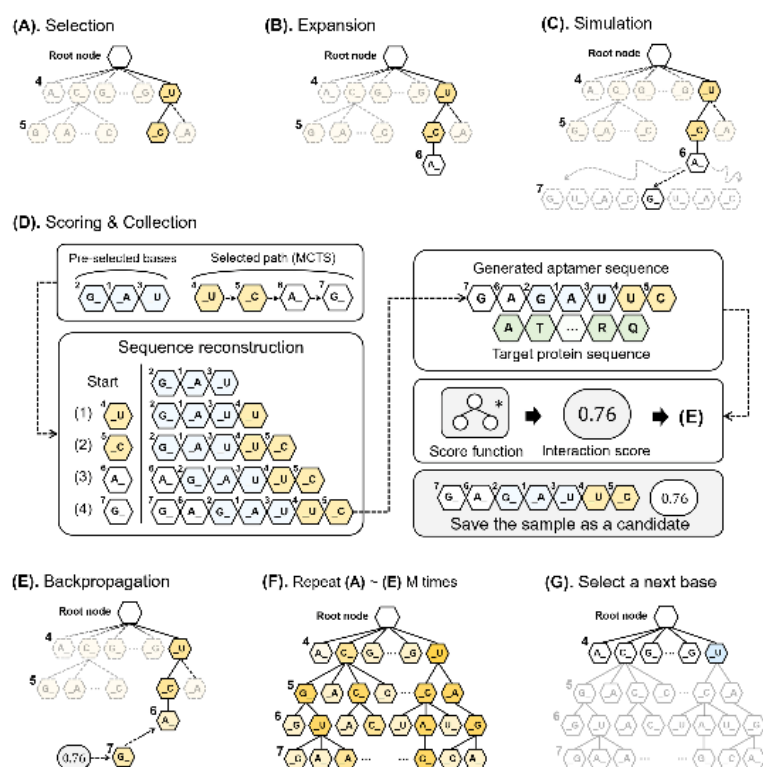


Figure 7 Details underlying the iterative forward sampling algorithm using MCTS to generate aptamer sequences⁹⁷

The goal was to generate aptamer candidates that could bind to this target, providing a potential tool for AD biomarker detection or therapeutic intervention. To achieve this, CeADAR employed a computational approach using the Apta-MCTS model, coupled with a Random Forest classifier optimized for API prediction.

The process began with a pre-trained Random Forest classifier¹⁰² on API data, specifically using a dataset derived from the benchmark study by Lee and Han (2019).¹⁰³ In the selection step (**Figure 7**), a path from the root to a leaf is chosen based on UCT (Upper Confidence bounds applied to Trees) scores, which are calculated as follows. The classifier’s performance was evaluated using several metrics¹⁰⁰: sensitivity (Sn), specificity (Sp), accuracy (Acc), Youden’s index (J), and the Matthews correlation coefficient (MCC). These metrics are defined in terms of true positives (TP), true negatives (TN), false positives (FP), and false negatives (FN), where TP and TN refer to correctly predicted API, and FP and FN refer to incorrect predictions.

¹⁰⁰ <https://www.aptagen.com/>

¹⁰¹ <https://sites.utexas.edu/aptamerdatabase/>

¹⁰² Breiman, L. *Random forests*. *Machine learning*, 45, 5-32 (2001).

¹⁰³ Lee, W., & Han, K. *Constructive prediction of potential RNA aptamers for a protein target* *IEEE/ACM transactions on computational biology and bioinformatics*, 17(5), 1476-1482 (2019).

$$UTC_{i,s_i,n_i,N_i} \stackrel{\text{def}}{=} \frac{s_i}{n_i} + C \times \sqrt{\frac{\ln(N_i)}{n_i}}$$

$$Sn = TP / (TP + FN)$$

$$Sp = TN / (FP + TN)$$

$$Acc = (TP + TN) / (TN + FP + FN + TP)$$

$$J = Sn + Sp - 1$$

The MCC is calculated using the following formula:

$$MCC = \frac{(TP * TN - FP * FN)}{\sqrt{(TP + FP)(TP + FN)(TN + FP)(TN + FN)}}$$

The final model, consisting of 173 decision trees, achieved the following performance metrics:

- MCC: 0.607
- Positive Predictive Value (PPV): 0.696
- Accuracy: 0.777
- Sensitivity (SN): 0.982
- Specificity (SP): 0.571
- Negative Predictive Value (NPV): 0.970
- Youden's Index (YD): 0.554

These metrics indicated an ability to predict API, which was crucial for generating high-affinity aptamer sequences. This metric is particularly valuable for imbalanced datasets because it takes into account all four components (TP, TN, FP, FN), unlike the F1-score which only considers precision and recall. The MCC ranges from -1 to 1, where 1 indicates perfect prediction, 0 indicates random guessing, and -1 indicates total disagreement between predictions and actual outcomes. A value of 0.607, as achieved in this study, indicates a strong level of confidence in the model's predictions. The classifier was trained to maximize MCC, ensuring reliable performance even when faced with imbalanced data.

To process the generation of candidate aptamers, the Apta-MCTS model integrates the Random Forest classifier into its sequence generation process. The model functions as follows:

Initialization:

- The target protein sequence (in this case, the beta-amyloid peptide (1-42) sequence) is provided along with the desired length of the aptamer candidates.
- A MCTS algorithm is used to explore the sequence space, where each node represents a nucleotide base (A, U, G, C) and paths from the root to leaves represent complete aptamer sequences.

Sequence Sampling via MCTS:

- The algorithm iteratively constructs sequences by selecting the most promising paths based on the Upper Confidence bounds applied to Trees (UCT) score, which balances exploration (trying new sequences) and exploitation (focusing on sequences with high predicted affinity).
- For each sequence generated, the Apta-MCTS model uses the pre-trained Random Forest classifier to score the potential interaction between the aptamer and the target protein.

Iteration and Optimization:

- The MCTS iterates over possible sequences, progressively refining the selection to maximize the interaction score predicted by the Random Forest model.

- At each iteration, the best sequence fragments are retained, and the search space is narrowed, reducing computational complexity.

Post-Processing:

- After generating a large pool of candidate sequences, the ViennaRNA package is used to predict the secondary structures of these aptamers. This step ensures that redundant sequences (those with identical secondary structures) are filtered out, retaining only unique and optimal candidates.
- The final list of sequences is sorted by their interaction scores, providing a ranked selection of aptamers for experimental validation.

Using this approach, CeADAR generated a set of candidate aptamer sequences with high interaction scores and secondary structures for the beta-amyloid peptide (1-42) sequence. The top candidates include:

1. **GAUGUAUUGUAACACUGCGUACUCCGCCGU**
 - **Interaction Score:** 0.806
 - **Secondary Structure:**(((.....)))..)
 - **Minimum Free Energy (MFE):** -2.6 kcal/mol
2. **AUGAUUAUACACUGCGUACUCCGCCUC**
 - **Interaction Score:** 0.801
 - **Secondary Structure:**(((.....)))....
 - **MFE:** -1.9 kcal/mol
3. **UGAUUUGUAACACUGCGUACUCCGCCGUU**
 - **Interaction Score:** 0.800
 - **Secondary Structure:**(((.....)))..)
 - **MFE:** -2.9 kcal/mol

These sequences represent preliminary candidates for binding the beta-amyloid peptide (1-42) target, offering a promising foundation for further refinement and validation through additional simulations. Moving forward, these results will serve as a baseline for continued exploration using more advanced models and computational strategies. In summary, through WP2, our comprehensive approach has not only enhanced our understanding of current computational methods for aptamer research but also set the stage for future improvements and deeper insights.

2.2 Aptamers' Selection

Aptamers are short single-stranded DNA (ssDNA) and hence are capable to form unique 3D structures which bind to different targets. The aptamer selection process (SELEX) is carried out by Novapech against AD specific biomarker proteins viz. A β 40, A β 42, NF-L and GFAP. The selection will be followed by characterization of selected aptamers by standard techniques of biomolecular interaction such as surface plasmon resonance (SPR), Bio-layer interferometry (BLI), etc. Aptamers thus capable to bind specific targets will work as recognition element in the different sensors systems mentioned ahead. In comparison to traditional antibodies, aptamers here, will provide increased flexibility in terms of handling & modification thus enhancing integration capability in sensors.

Before starting the selection, Novaptech has performed literature search to find the already reported aptamers against A β ₄₀ and A β ₄₂ peptides, Tau proteins phosphorylated at specific sites, GFAP and NFL. The literature aptamers are shown in **Table 3**: Literature Aptamers for AD protein *biomarkers*.

Table 3: Literature Aptamers for AD protein biomarkers.

Name	Target	Binding affinity	Reference
RNV95	A β ₄₀ oligomer	50–400 nM	Chakravarthy et al., 2018 ¹⁰⁴
T-SO508	A β ₄₀ oligomer	25 nM	Tsukakoshi et al., 2012 ¹⁰⁵
A β 7-92-1H1 (A β -Apt)	A β ₄₂ mono-/ oligo-mers	63.4 nM/ 53.3 nM	Zheng et al., 2020 ¹⁰⁶

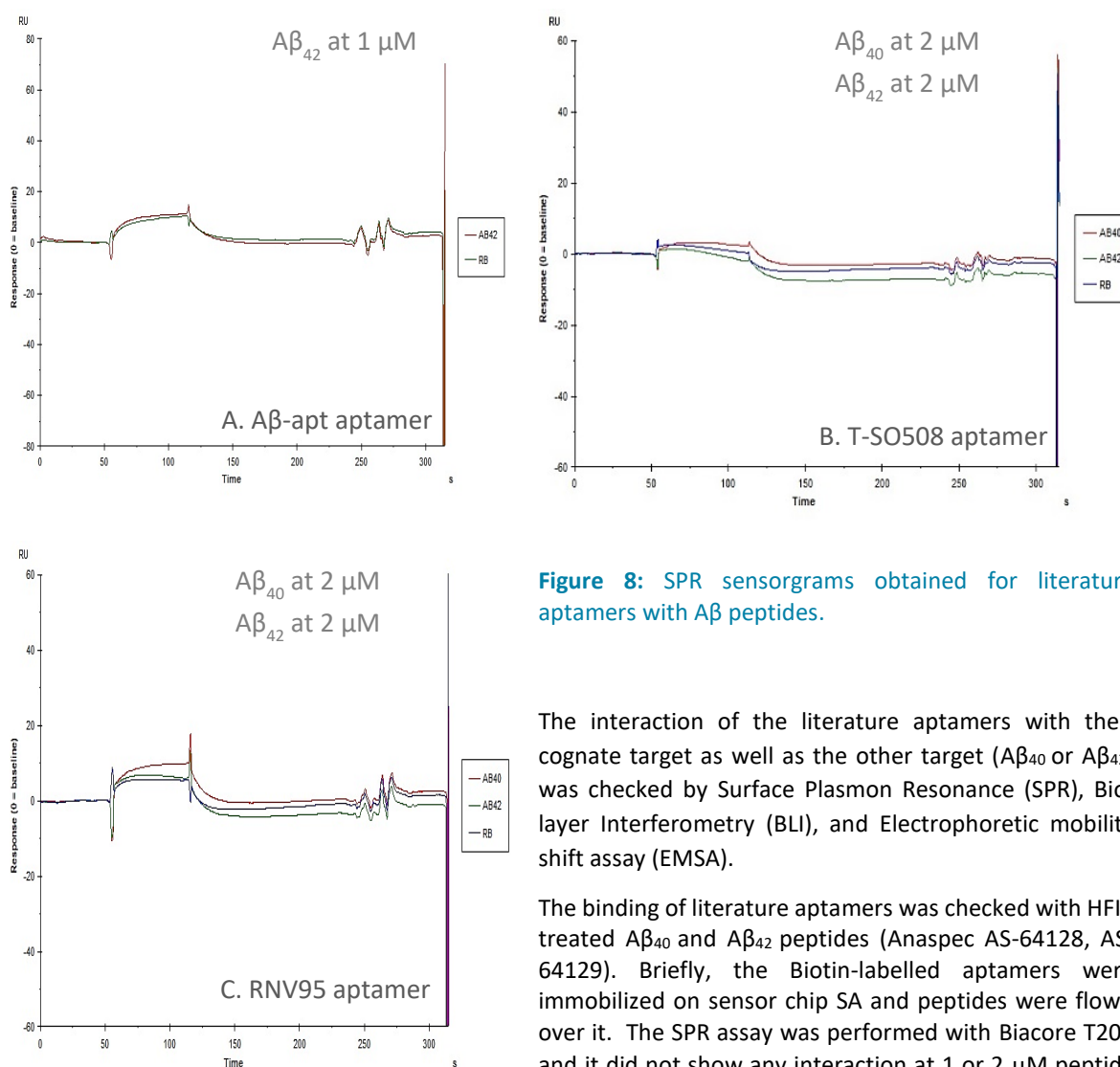


Figure 8: SPR sensorgrams obtained for literature aptamers with A β peptides.

The interaction of the literature aptamers with their cognate target as well as the other target (A β ₄₀ or A β ₄₂) was checked by Surface Plasmon Resonance (SPR), Bio-layer Interferometry (BLI), and Electrophoretic mobility shift assay (EMSA).

The binding of literature aptamers was checked with HFIP treated A β ₄₀ and A β ₄₂ peptides (Anaspec AS-64128, AS-64129). Briefly, the Biotin-labelled aptamers were immobilized on sensor chip SA and peptides were flown over it. The SPR assay was performed with Biacore T200 and it did not show any interaction at 1 or 2 μ M peptide concentrations as shown in **Figure 8**.

¹⁰⁴ Chakravarthy, M. et al., [Development of DNA aptamers targeting low-molecular-weight amyloid- \$\beta\$ peptide aggregates in vitro](#) Chem. Commun. 54, 4593 (2018).

¹⁰⁵ Tsukakoshi, K. et al., [Selection of DNA aptamers that recognize \$\alpha\$ -synuclein oligomers using a competitive screening method](#) Anal. Chem. 84, 5542 (2012).

¹⁰⁶ Zheng, Y. et al., [Development of DNA Aptamer as a \$\beta\$ -Amyloid Aggregation Inhibitor](#) ACS Appl. Bio Mater. 3, 8611 (2020).

Next, the interaction was studied using BLI and after thorough investigation, it was found that aptamers RNV95 and TSO508 were not able to recognize neither $A\beta_{40}$ nor $A\beta_{42}$ peptides (HFIP treated peptides). Interaction assays for BLI were performed on Octet R8 platform. The aptamer $A\beta$ -apt showed an interaction with HFIP treated $A\beta_{40}$ peptide and the binding kinetics is shown in the Figure 9:. Briefly, $A\beta$ -apt was immobilized on the SA sensors (for BLI) and interaction was measured in range of 125 nM to 1000 nM $A\beta_{40}$ peptide. A concentration dependent interaction $A\beta$ -apt was observed with $A\beta_{40}$ peptide. The results were analysed after blank subtraction using 1:1 binding model. The equilibrium dissociation constant for this aptamer-target pair is 43.2 nM and a R^2 value of 0.9988 indicated a good fit (**Figure 9**).

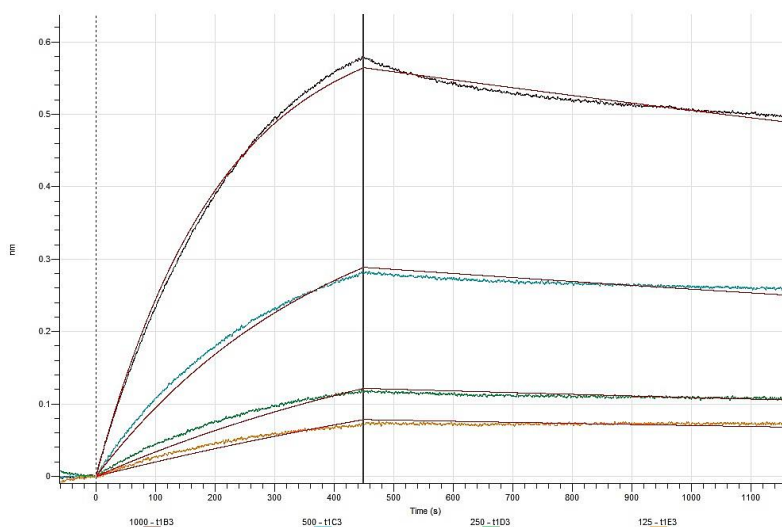


Figure 9: Binding/affinity evaluation of literature aptamer $A\beta$ -apt with $A\beta_{40}$ peptides by BLI. The responses are maroon- 1000 nM, blue 500 nM, green 250 nM, and orange is 125 nM. Continuous lines correspond to curve fittings.

In an attempt to reproduce the results, the same experiment was repeated it was found that both the peptides bound to SA sensor non-specifically. The binding of the peptides was too strong as indicated by blank subtracted graph in **Figure 10**.

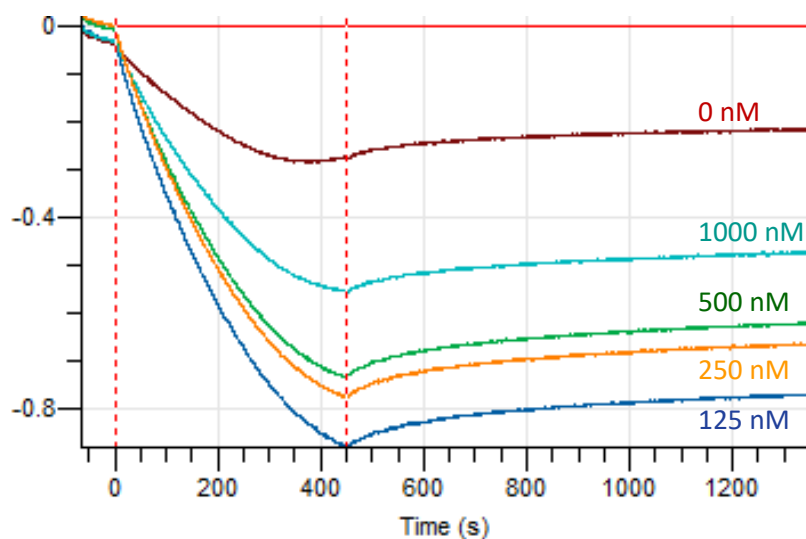


Figure 10: Processed data showing the binding signals after background subtraction. The different lines are- the maroon line- 0 nM, aqua line- 1000 nM, green line 500 nM, orange line 250 nM, and blue line indicates 125 nM of $A\beta_{42}$ peptide. Here the negative graphs were obtained because background binding was subtracted it was higher than binding with aptamer.

Results could not be replicated using the same peptide lot which could be an indication of a change in the peptide structure over time. Hence the binding obtained was inconclusive. The electrophoretic mobility shift assay was also negative: no effect of the peptides was detected on the mobility of aptamers on an agarose gel. The electrophoretic mobility shift assay was also no different and the binding could not be confirmed with it either.

Below is the summary/overview of aptamer selection process for all the biomarkers:

A β ₄₀ and A β ₄₂ peptides: As literature aptamers' binding was inconclusive, a new selection was started against both peptides which unfortunately did not show any enrichment and did not yield aptamer candidates. Aptamer selection depends entirely on the target structure and form and hence the target must remain in the same form throughout the selection. Since the structure of these peptides is a major concern, we plan to launch any new selection once we receive some conclusive information/find some ways via interaction with other consortium members to maintain the structure/form of these peptides.

Tau: Commercial availability issues with the target. The required quantity and desired form of protein is not available commercially. The desired form is available with certain suppliers mentioned below:

GENEMEDI (GMP-h-p-tau231-Ag02) where the price is \$28000 per mg and one branch of aptamer selection and characterization could consume around 200-300 μ g of protein making it hard to visualise.

pTau217 is also available as standard protein with ELISA based detection kits. These kits contain only a few picograms of standard protein and it as well, will not be sufficient for aptamer selection. The suppliers of ELISA kits include [Quanterix](#)[®], [ThermoFisher Scientific](#), [Fujirebio](#), etc. Unfortunately, these options cannot be explored because even procuring plenty of kits would not suffice the required pTau217 amount.

NFL: Selection and sequencing for NF-L are completed and the NGS data obtained is being analysed to obtain information about motifs, clusters and secondary structure. Briefly, the selection was carried out in four branches using two different aptamer libraries. The quality parameters such as, pool PCR amplification, single-stranded DNA generation were found to be satisfactory.

After NGS analysis, representative sequences will be synthesised for biophysical characterisation. The characterisation of aptamer candidates is expected to be over by end of September 2024. Besides this, a new selection is also currently under progress for this biomarker using different libraries and procedures.

GFAP: Selection and bio-informatic analysis of the selected pools are completed. To summarize the aptamer selection against GFAP:

1. The selection was carried out in three parallel branches where each branch represents a condition using an aptamer library, hence three conditions, A, B and C represent selections starting of different libraries. In the 10 selection rounds performed, the quality and the quantity of pools produced at the successive rounds remained satisfactory and positive.
2. Pools were well and progressively enriched under the applied selection pressure. The enrichment was monitored by sequencing of library and pools of rounds 6, 9 and 10 for all conditions. The enrichment obtained is shown in **Figure 12**.
3. The motif prediction analysis of evolved pools (Next Generation Sequencing analysis) indicated that the most represented motifs were G-repeats. We could also see the evolution

of some T and C rich motifs for two of selection conditions (A and B) as shown in the **Figure 12**. Further the evolutionary profile was also studied by clusterization and secondary structure prediction.

4. On the basis of presence of motif sequences, clustering and secondary structures, the representative sequences (**Table 4**) were selected for further biophysical characterization. At current, Novaptech is awaiting the delivery of synthesized sequences to proceed for the biophysical characterisation using SPR and BLI. The characterisation of the selected aptamer candidates is expected to be over in the forthcoming weeks.
5. Besides this, two new selections are also currently under progress for this biomarker using different libraries and procedures.

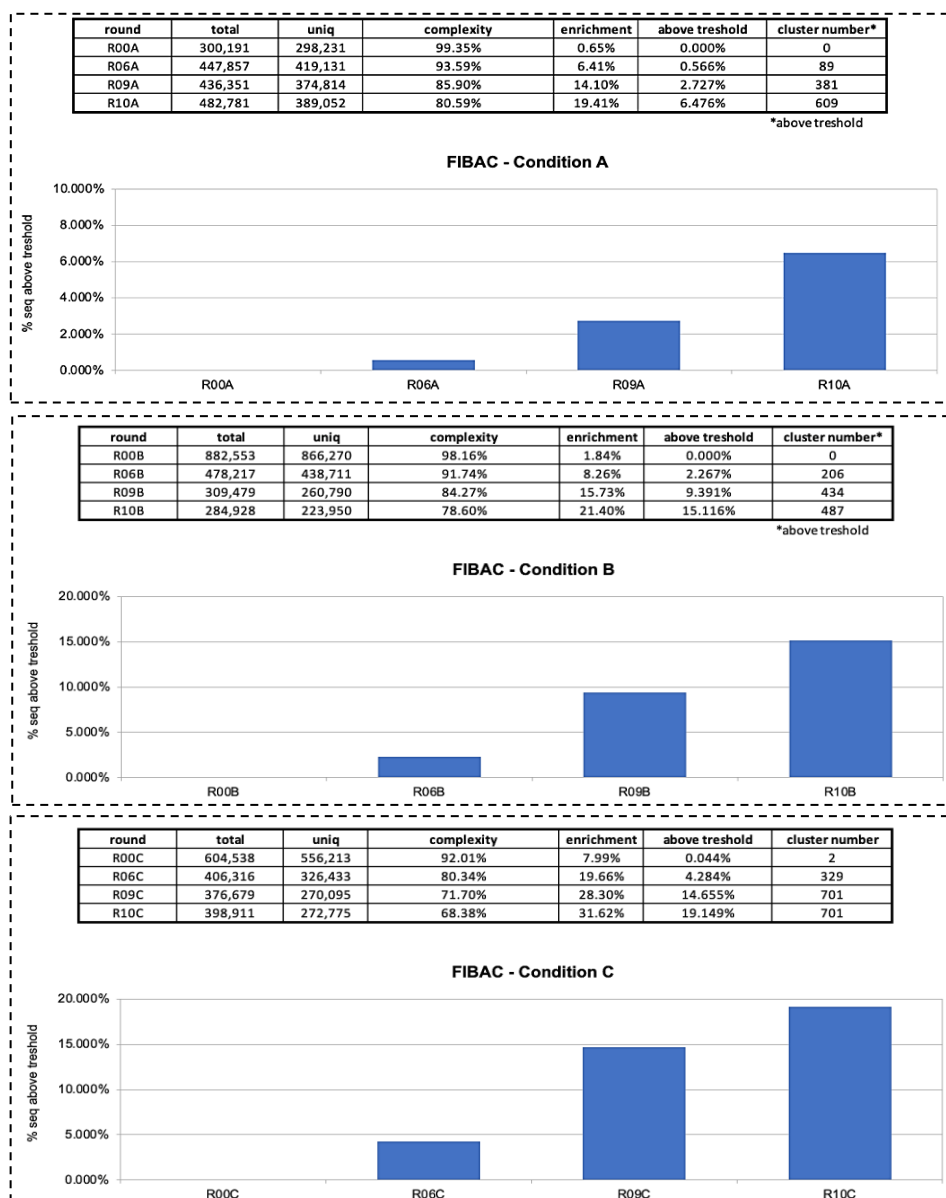


Figure 11: Evolution of the pool from R06 to R10.

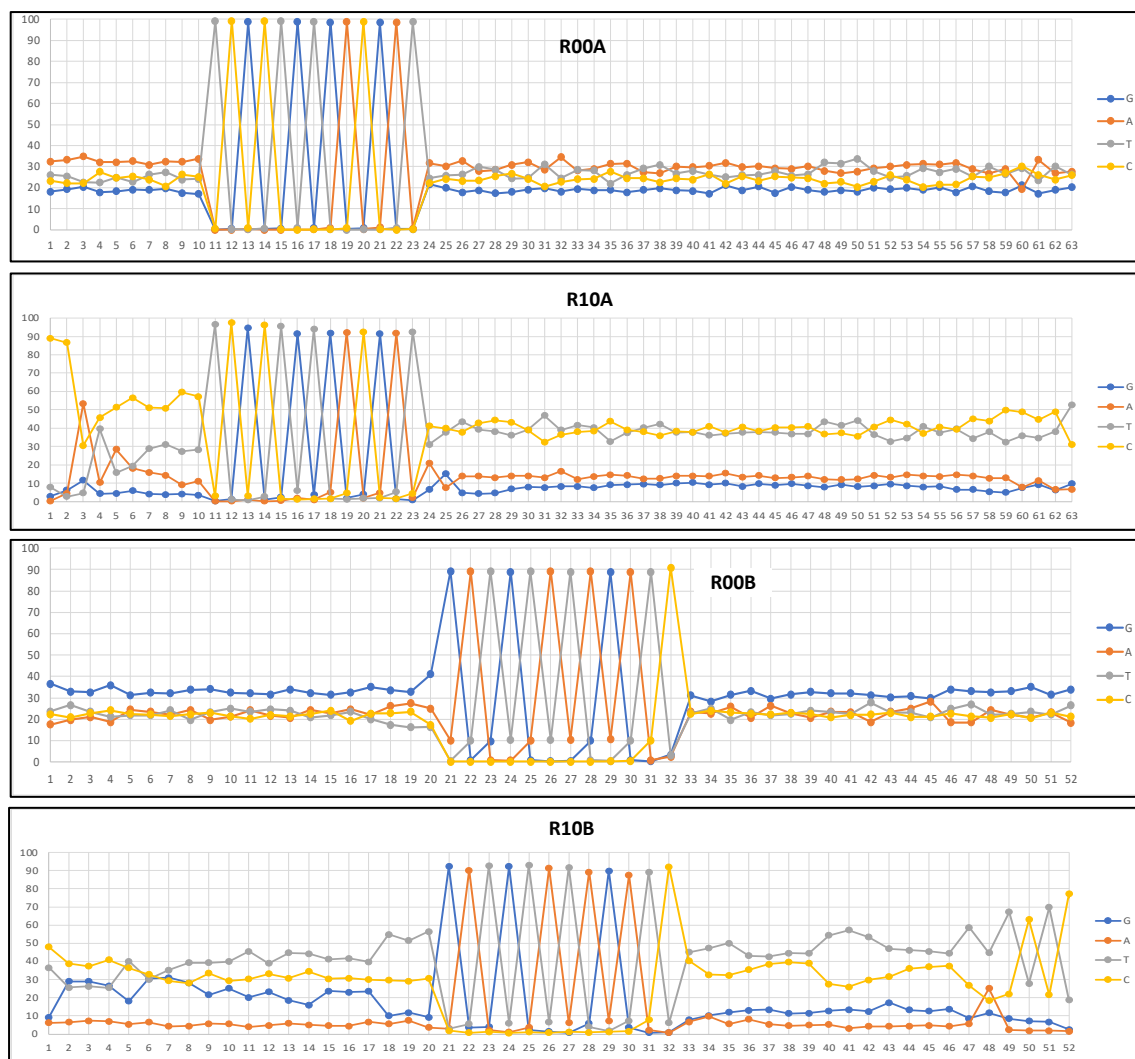


Figure 12: Percent T and C composition of selection round 10 for conditions A and B. For comparison, the starting aptamer library compositions for both conditions have been shown as R00A and R00B.

Table 4: Sequences for biophysical characterisation after selection against GFAP.

FIB001A	GCAGTAATTGATCCTATGGTTGGGGGGGCTCGCTGTGACGATATTTGGGGCGGGCGGGTTTGTTCAGATCTAACTTCGCTATTA CGTGACACTACC
FIB004A	GCAGTAATTGATCCTATGGCCATCCCTCCTCGCTGTGTTCTCCCCTACCCCGTTCATATCTCTTTCCTCCCATGCGCTATTACGTGACAC TACC
FIB007A	GCAGTAATTGATCCTATGGCCATATCCCTCCTCGCTGTGACGATCCCTTCTCTGTTGTACCGCCTTCCCCCGCCCTTATGCTATTACGTG ACACTACC
FIB010A	GCAGTAATTGATCCTATGGCTGCCATGGGTGCTGTGACGATGAATACTATGCCCTGCATTATCCAGAGGGTTAAATGATGCGCTATTAC GTGACACTACC
FIB042A	GCAGTAATTGATCCTATGGCCCTTACCTCGCTTACGATCGTCACCATGTCCCGATACACTTGCTTCTCACTGCTATTACGTGACACTA CC
FIB002B	AGCCTCGTCTGTTCTCCCTGGGTGGGTGGGTGGGTCTGATGTATAGATCTTCTTATTGCCGTCTCTCGAGATAGTCAGTGGCAGCT
FIB003B	AGCCTCGTCTGTTCTCCCTGGGTGGGGGCTGGTCTTTGATGTATAGATCGCCGGTGGGGGGTGGTTTCGAGATAGTCAGTGGCAGCT
FIB004B	AGCCTCGTCTGTTCTCCCTCTCTGTTTTACCCTCTTGATGTATAGATCCATCCCTCCTTCTATCTCGAGATAGTCAGTGGCAGCT
FIB011B	AGCCTCGTCTGTTCTCCACGTTGAGTCTTAGTCTTGATGTATAGATCCCGGATAGACGGCTTCTCGAGATAGTCAGTGGCAGCT
FIB012B	AGCCTCGTCTGTTCTCCCTGCGTTGCATATTTCACTGATGTATAGATCTTGGTTGGTTGGTCTGGTAGAGATAGTCAGTGGCAGCT
FIB013B	AGCCTCGTCTGTTCTCCCTCCGAGCCGAACCGGATTAGATGTATAGATCTTAAGTATTCATACGAGACGGAGATAGTCAGTGGCAGCT
FIB001C	GCTTAGGACGAATTACTCTCTCGCATATTGGTTTGGTTGGTCTGGTCTGATGCTCCCTACTAACAGCGTTCTGGATGAT
FIB002C	GCTTAGGACGAATTACTCTCTGGGTGGGAGGGAGGGGGTGGTAGGGGTCTTCTCTGCTAACAGCGTTCTGGATGAT
FIB004C	GCTTAGGACGAATTACTCTCACTGCTTTTCTTATAGGGTTGGCTTGGGTCTGGCACTAACAGCGTTCTGGATGAT
FIB006C	GCTTAGGACGAATTACTCTCAGGACGCTCCACCTTAGTGGATGATACTCACTCTTTGACTAACAGCGTTCTGGATGAT
FIB007C	GCTTAGGACGAATTACTCTCAGGGTAACACTGACACTCGATGCTAACAGGATAGGAGTCTAACAGCGTTCTGGATGAT
FIB011C	GCTTAGGACGAATTACTCTTGGGGGGAGGGAGGGGGAGGTGGATGGAATACTCGTTGCTAACAGCGTTCTGGATGAT

We proceeded to the evaluation of all the candidates listed in **Table 4** by SPR. To this end these oligonucleotides were immobilized on the streptavidin sensor chip by hybridization to a complementary biotinylated capture oligonucleotide. Then a GFAP solution was injected over the chip at different concentrations in the selection buffer. In a second step the buffer only was injected. The starting libraries were used as a negative control. The resonance signal was recorded during the association and dissociation phases.

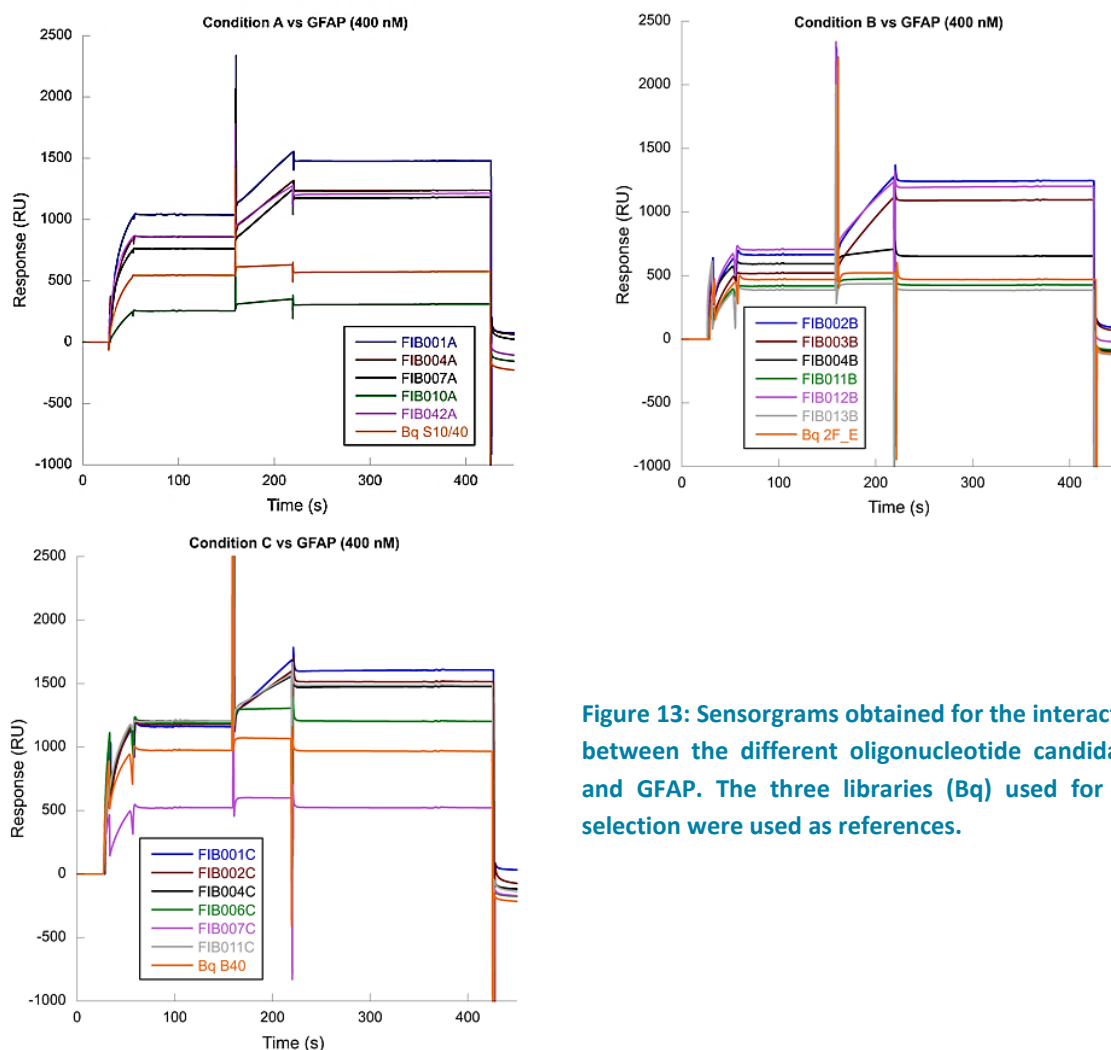


Figure 13: Sensorgrams obtained for the interaction between the different oligonucleotide candidates and GFAP. The three libraries (Bq) used for the selection were used as references.

The sensorgrams obtained at 400 nM GFAP are shown in **Figure 13**. Several candidates generated a strong resonance signal characterized by a very fast association and a slow dissociation. Similar results were obtained at 200 nM GFAP. For 2 of the candidates we performed a kinetic analysis, i.e. successive evaluation of the binding at 5 different concentrations (**Figure 14**). A fit according to a 1:1 model complex allowed the determination of K_d s in the low nanomolar range for these 2 candidates. In conclusion we obtained strong aptamers for GFAP.

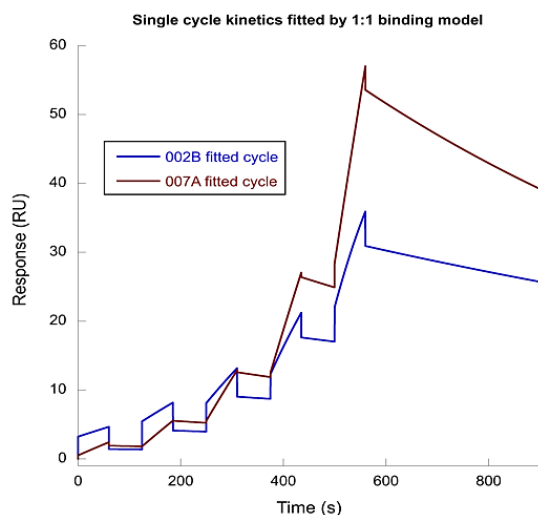
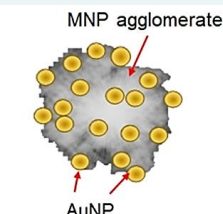
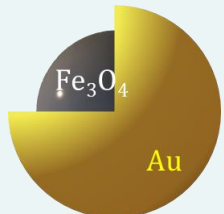




Figure 14: SPR analysis of the interaction between candidates FIB002B and FIB007A.

2.3 Nanoparticles' Design & Synthesis

As part of WP2, AUTH (Aristotle University of Thessaloniki) is responsible for the design and synthesis of tailor-made MNPs to be conjugated with DNA aptamers. In this framework biphasic (Magnetite/Au) MNPs, with variable size composition, morphology, are synthesized,^{107,108,109} characterized and adequately characterized before and after the conjugation with DNA.¹¹⁰ Au component serves as a conjugation site for the selected DNA aptamers, while the magnetite component acts as a natural magnet to enhance aptamer concentration when exposed to an external magnetic field. It enables precise flow control and signal amplification upon request. To date, AUTH has successfully synthesized and structurally characterized three distinct different biphasic nanostructure architectures as depicted in **Table 5**. The role of the magnetic counterpart is to enhance sensitivity and reliability via sample purification, minimalization of non-specific signals, and flow regulation during various stages of bioassays, such as bioreceptor incubation, purification, recognition, and signal acquisition. Au part serves as an electrochemical signal enhancer since it is already successfully implemented in biosensing techniques for detecting blood biomarkers like A β 40, A β 42, and p-Tau, exhibiting good selectivity, specificity, fast response, and low limits of detection (LOD), across different stages of AD. Au specimen is the reference sample to determine conjugation efficiency (described in the following section).

Table 5: Nanoparticle formulations composed of Au/Fe₃O₄ synthesized within WP2 framework and the corresponding synthetic methodologies.

Au-decorated MNPs	Core/shell	Yanus particles	Au reference
 <p>MNP agglomerate AuNP</p>	 <p>Fe₃O₄ Au</p>	 <p>Au Fe₃O₄</p>	 <p>Au</p>
Ref. 107	Ref. 108	Ref. 109	Ref. 111

The successful synthesis of the desired nanoparticles was confirmed through a series of characterization techniques. X-ray Diffraction (XRD) patterns exhibited characteristic peaks corresponding to the crystal structure of the nanoparticles, confirming their phase purity (**Figure 16** Left Figure). Transmission Electron Microscopy (TEM) images revealed uniform particle size and morphology consistent with the intended design.

XRD patterns showed distinct diffraction peaks corresponding to Fe₃O₄ and Au, affirming the successful synthesis of the designated nanoparticles (Left figure). Distinct diffraction peaks corresponding to Fe₃O₄ (black) and Au (gold) are observed, indicating the presence of the two phases and confirming the successful incorporation of both components in the nanoparticles. TEM images (Right side graphs of **Figure 16**) revealed well-defined nanoparticles with a uniform distribution. Top image shows how Au -Fe₃O₄ NPs are dispersed in the IP6 matrix. The presence of IP6 (**Figure 16**-Top right image) as a stabilizer and a bridging agent assembles Fe₃O₄ nanoparticles (NPs) into a magnetic

¹⁰⁷ Miyazaki et al. [Gold conjugated-magnetite nanoparticles for magnetic concentration towards reproducibility and repeatability of SERS measurements](#). *Colloids Surf. A Physicochem.* 671: 131661 (2023).

¹⁰⁸ Zhou, H. et al. "Ultrasensitive DNA monitoring by Au-Fe₃O₄ nanocomplex." *Sensors and Actuators B: Chemical* 163.1: 224-232 (2012).

¹⁰⁹ Garanina, A. S. et al. [Bifunctional magnetite-gold nanoparticles for magneto-mechanical actuation and cancer cell destruction](#). *Magnetochemistry* 8.12: 185 (2022).

¹¹⁰ Gamboa J. et al., [Aptamers for the Delivery of Plant-Based Compounds: A Review](#) *Pharmaceutics*, 16, 541 (2024).

¹¹¹ J. Dong et al., [Synthesis of precision gold nanoparticles using Turkevich method](#) *KONA Powder and Particle Journal* 37, 224-232 (2020).

network nanoassembly, composed from a Fe_3O_4 core decorated with Au nanoparticles. The center and bottom images in right panel of

Figure 15 illustrate the core-shell structure of the synthesized Fe_3O_4 -Au nanoparticles (NPs). These images visually depict the unique architecture where the magnetite (Fe_3O_4) forms the core, providing magnetic properties, while the gold (Au) forms the outer shell, serving as the site for aptamer conjugation and enhancing the electrochemical signal. This core-shell design is essential for the dual functionality of the NPs, combining magnetic manipulation with high-affinity biomarker detection, which is crucial for the efficiency of the bioassay process.

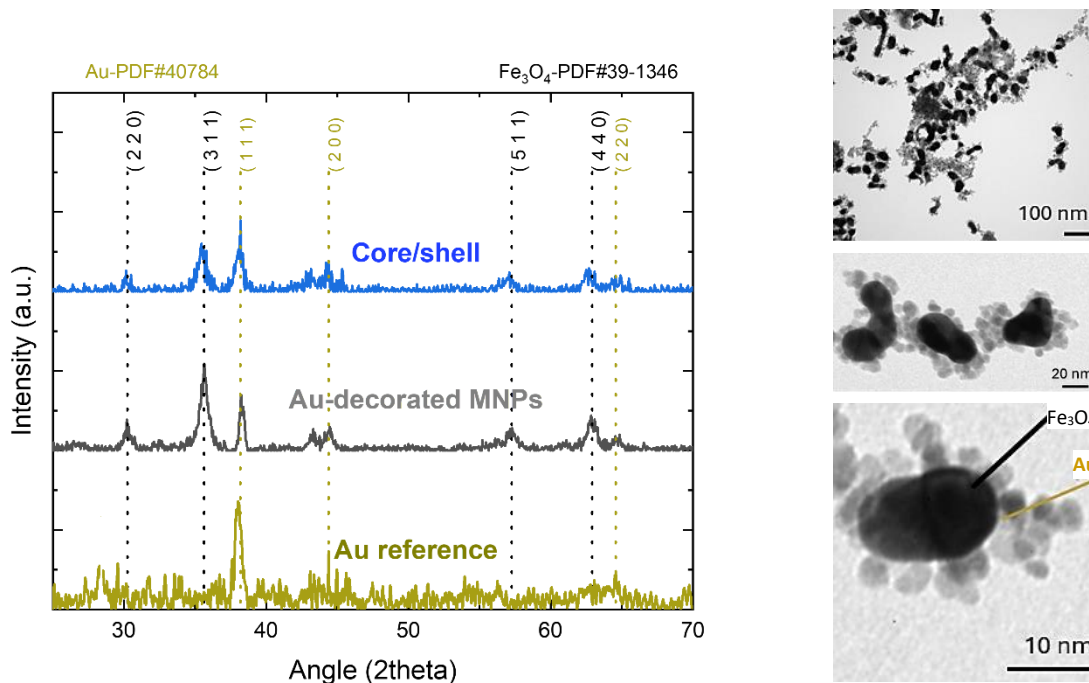


Figure 15: Left figure: X-ray Diffraction (XRD) pattern of the synthesized nanoparticles. Right figure: (top): Transmission Electron Microscopy (TEM) image showing agglomerates of magnetic nanoparticles (MNPs), specifically Fe_3O_4 , with gold nanoparticles (Au NPs) decorating their surface, forming an inositol hexaphosphate (IP6) network. (Center and Bottom): TEM images of core-shell nanoparticles, with Fe_3O_4 as the core and Au as the shell (Fe_3O_4 @Au NPs).

Furthermore, Dynamic Light Scattering (DLS) analysis (**Figure 16:**) indicated a narrow size distribution, corroborating the TEM findings. The size distribution indicates a mean average size of 1122 nm, 15.7 nm and 78 nm for Au decorated MNPs ($\text{Au}-\text{Fe}_3\text{O}_4$) (a), core/shell (Fe_3O_4 @Au) (c) and Au reference NPs (e), respectively. In the case of Au decorated MNPs, since the nanoparticles are embedded in the citric acid matrix, the observed sizes are consistent with the expected dynamic light scattering measurements. The zeta potential of the Au decorated nanoparticles was determined to be -49 mV (b), whereas the zeta potential of core/shell and Au reference nanoparticles was found to be more negative, measured at -77 mV (d) and -64 mV (f), respectively. Zeta potential is a physical property which is exhibited by any particle in suspension. It facilitates optimization of suspension formulations and predicts interactions with surfaces. Knowledge of the zeta potential reduces the time needed to produce trial formulations and aids long-term stability. The negative sign of ZP denotes the highest

bio-interactions compared with other formulations with less negative charge and/or positive surface charge due to electrostatic interactions.

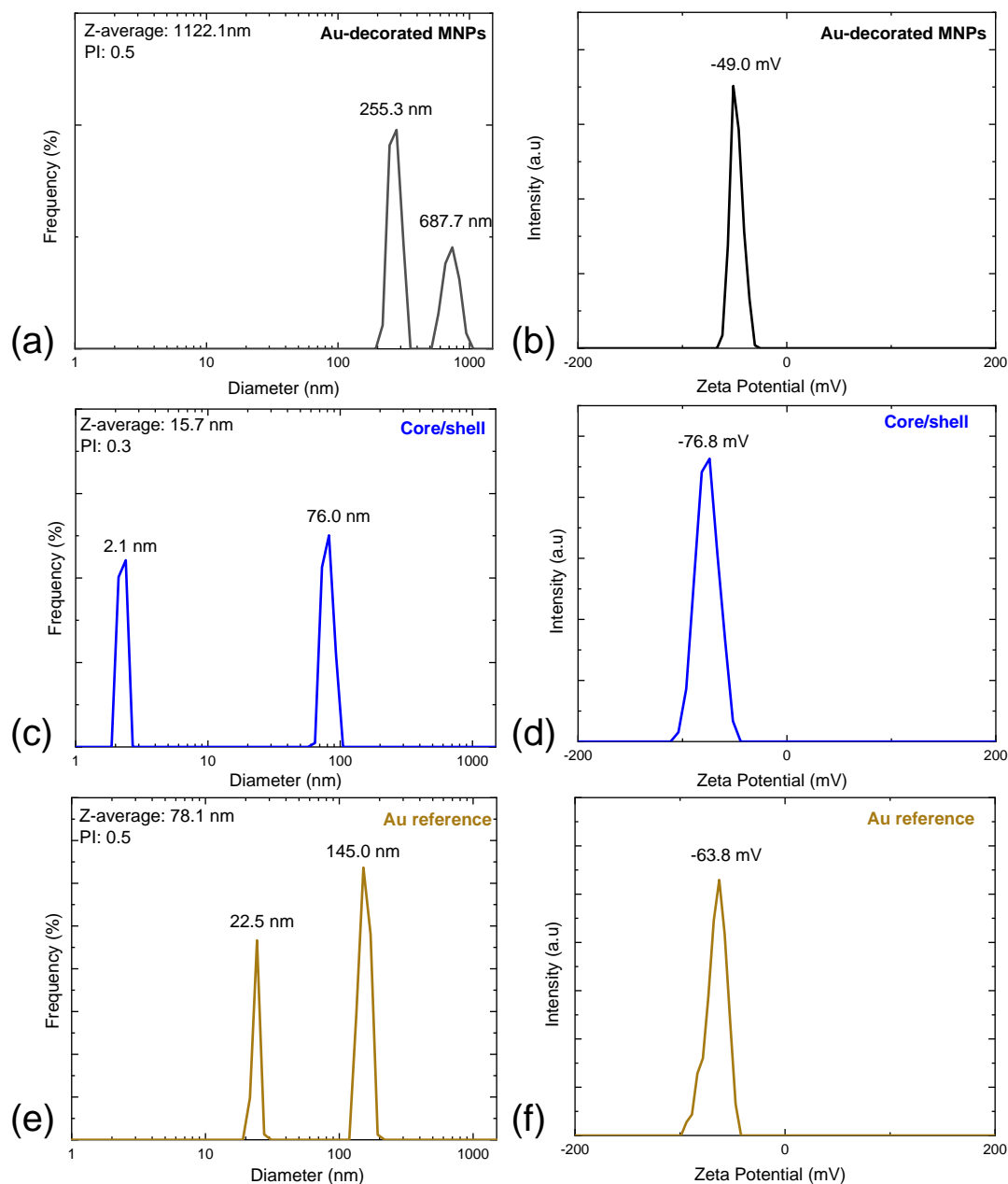


Figure 16: Dynamic Light Scattering (DLS) of Au decorated MNPs (a), core/shell (c), Au reference (e), and ζ -potential analysis of the synthesized nanoparticles (b), (d) and (f) respectively.

Additionally, the magnetic properties of the nanoparticles were assessed using Vibrating Sample Magnetometry (VSM), which demonstrated magnetic behavior in line with the expected characteristics of the synthesized material. The room temperature hysteresis loops in **Figure 17**: demonstrate the typical ferrimagnetic behavior of Fe_3O_4 with a saturation magnetization of 40 emu/g and 49 A m²/kg for Au decorated MNPs (AuFe_3O_4) and core/shell ($\text{Fe}_3\text{O}_4@Au$) NPs, respectively. Based on the bulk magnetization value of Fe_3O_4 being approximately 90 A m²/kg, the magnetite content in the nanoparticles is estimated to be around 46% and 56% for Au decorated MNPs and core/shell NPs, respectively.

These results collectively validate the successful synthesis of the nanoparticles with the designated specifications.

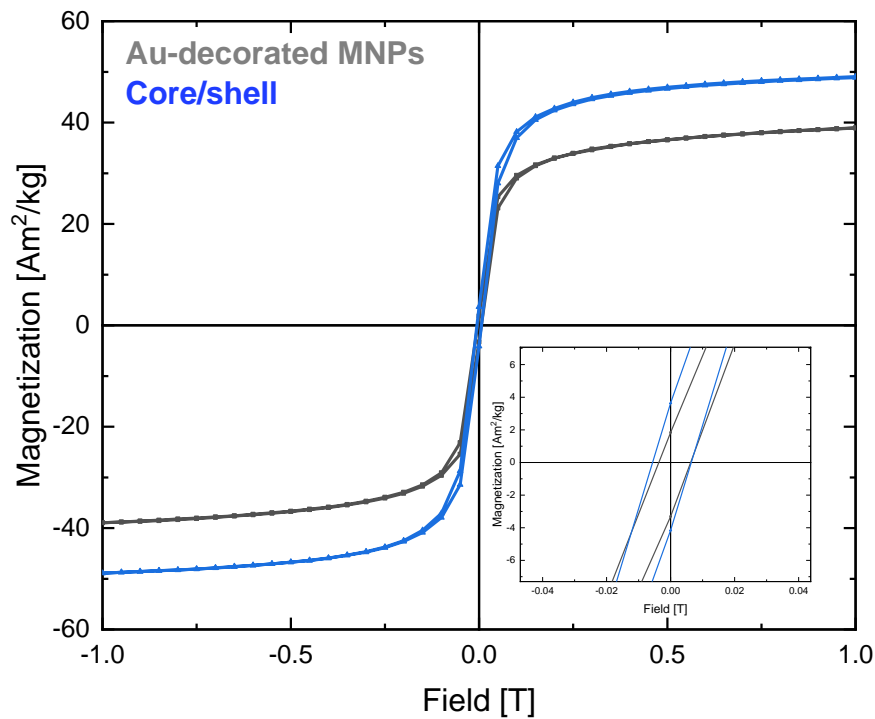


Figure 17: Hysteresis loop of Au-Fe₃O₄ nanoparticles: Au decorated MNPs (grey) and core/shell NPs (blue), as measured by Vibrating Sample Magnetometry (VSM).

2.4 Conjugation of NPs with Aptamers

The conjugation with aptamers will be achieved by using well-established cross-linking methodologies, aiming to (i) provide an adaptable and scalable solution that can easily be adjusted to different biomarkers; and (ii) target a 1 (MNP): 1 (aptamer) ratio to be achieved, further increasing the selectivity and specificity capability per biomarker. Conjugation of thiol-modified aptamers on MNPs will be evaluated with alternative protocols to validate enhanced signal and performance i.e. overnight freezing,¹¹² amino-modified aptamers with EDC/NHS chemistry on carboxyl-modified NPs,¹¹³ or APTES/glutaraldehyde chemistry on OH-modified NPs.^{114,115} To evaluate the conjugation efficiency, FAM-modified fluorescent aptamers will be employed. After conjugation, aptamers will be detached from the MNPs and quantified with fluorometry. Furthermore, the conjugation of aptamers on MNPs will be evaluated through the determination of electrophoretic mobility on agarose electrophoresis and the spectrophotometric analysis of the MNPs. Aptamer-modified MNPs are expected to retain or even increase their absorbance, or present slight upshifts at their absorbance maxima.

Conjugation Experimental Protocol

Thrombin has previously been suggested as a possible pathological mediator in AD as it is associated to the characteristic hallmarks of AD-related pathology.¹¹⁶ Thrombin has been detected in senile plaques and in neurofibrillary tangles characteristic of this disease¹¹⁷ and levels of both thrombin and the thrombin receptor PAR-1 are elevated in AD.¹¹⁸ A variety of thrombin aptamers have been reported, with TBA1 being the most widely used (5'-GGTTGGTGTGGTTGG-3'). TBA1 binds to the fibrinogen-recognition exosite of thrombin with a $K_d \approx 100$ nM. Thrombin aptamers fold to form G-quadruplex structures, in the process of recognition with thrombin.¹¹⁹ Based on the optical properties of gold nanoparticles (AuNPs), an assay platform was developed to realize easy but efficient detection of thrombin with ultrahigh sensitivity.¹²⁰ Simultaneously using TBA1 as the detection probe and another aptamer for thrombin, TBA2, as the capture probe, a click chemistry-based electrochemical sensor for the simple and fast detection of thrombin was manufactured, with great applicability potential.¹²¹

Herein, due to the numerous applications employing thrombin aptamer and the potential employment of thrombin to AD, we decided to perform the conjugation reference experimental protocol on the potential of binding TBA1 on gold nanoparticles (Au NPs) as follows:

a. Conjugation of thiol-aptamer on MNPs

The conjugation phenomenon is extremely dependent on the type of the employed aptamer, the reaction pH, and temperature. To attach negatively charged DNA to negatively charged Au, a freezing-

¹¹² B. Liu and J. Liu [Freezing Directed Construction of Bio/Nano Interfaces: Reagentless Conjugation, Denser Spherical Nucleic Acids, and Better Nanoflakes](#), *J. Am. Chem. Soc.* 139, 9471–9474 (2017).

¹¹³ F. Odeh et al., [Aptamers Chemistry: Chemical Modifications and Conjugation Strategies](#), *Molecules* 25, 3 (2020).

¹¹⁴ Gunda N. S. K. et al., [Optimization and characterization of biomolecule immobilization on silicon substrates using \(3-aminopropyl\)triethoxysilane \(APTES\) and glutaraldehyde linker](#) *Applied Surface Science* 305, 522–530 (2014).

¹¹⁵ Sypabekova M. et al., [Review: 3-Aminopropyltriethoxysilane \(APTES\) Deposition Methods on Oxide Surfaces in Solution and Vapor Phases for Biosensing Applications](#), *Biosensors* 13, 36 (2023).

¹¹⁶ Grammas, P., Martinez, J.M., 2014. [Targeting thrombin: An inflammatory neurotoxin in alzheimer's disease](#). *J. Alzheimer's Dis.* 42, S537 - S544 (2014).

¹¹⁷ Arai, T. et al., [Thrombin and prothrombin are expressed by neurons and glial cells and accumulate in neurofibrillary tangles in Alzheimer disease brain](#). *J. Neuropathol. Exp. Neurol.* 65, 1, (2006).

¹¹⁸ Krenzlin, H. et al., [The importance of thrombin in cerebral injury and disease](#). *Int. J. Mol. Sci.* 17(1), 84 (2016).

¹¹⁹ Sun, H. et al., [Aptamer-Based Sensors for Thrombin Detection Application](#) *Chemosensors* 10(7), 255 (2022).

¹²⁰ Li, J. et al., [Colorimetric Detection of Thrombin Based on Intensity of Gold Nanoparticle Oligomers with Dark-Field Microscope](#) *ACS Sustain. Chem. Eng.* 6, 5, 6738–6745 (2018).

¹²¹ Liu, Q. et al., [Click chemistry-based aptasensor for highly sensitive electrochemical detection of thrombin](#) *Anal. Methods*, 9, 3825-3830 (2017).

directed conjugation of DNA aptamers on gold nanoparticles was implemented, as it was proven adequate for various Au NPs, from 5 to 100 nm in diameter, and with several thiolated DNA sequences.¹²² The first attempt was to conjugate thrombin aptamer to Reference Au NPs. The thrombin aptamer was TBA1 (5'-GGTTGGTGTGGTTGG-3') and Au NPs were synthesized, as described in previous section.¹¹¹ The concentration of AuNPs was calculated spectrophotometrically at 520 nm using a theoretical extinction coefficient (assuming $\epsilon = 2.4 \times 10^8 \text{ M}^{-1} \times \text{cm}^{-1}$ for a diameter of 12 nm of Au reference NPs), and with the Lambert-Beer law ($A = \epsilon cl$). As a result, the concentration of Au reference NPs was calculated at 2.346 nM. Au NPs are mixed with SH-Aptamer at various aptamer concentrations (0.6 μM , 0.9 μM , 1.19 μM , 2.34 μM , 4.69 μM) at a final volume of 500 μl in sterile centrifuge tubes. The tubes were kept at -20°C for at least 2 hours and then thawed at room temperature (RT) and centrifuged to discard the unbound aptamers at 13,500 rpm, for 15 min, at 4°C . Finally, aptamer-Au NPs were washed three times with Tris-EDTA buffer, pH 8 (TE), and stored in double distilled water (d.d. H_2O), at 4°C , in the dark. Thawing after at least 2 hours of freezing was enough to produce stable aptamer-gold nanoconjugates, with a density 20-30% higher than the one verified by the typical salt-aging method.

b. Determination of bound aptamer

To detect and measure the amount of bound 6-Carboxyfluorescein (FAM)-modified thrombin aptamers on Au NPs, aptamer-AuNP nanoconjugates were treated with 0.1 M DTT for 5 min at 50°C , followed by 1 h incubation at RT, in the dark.

Surface modification of Au NPS was achieved using thiolate reaction and immobilization of thiol-labeled 15-mer thrombin aptamer that were previously modified with FAM (**Figure 18:a**). The immobilization of thiol-aptamer was optimized by monitoring the fluorescence intensities (Excitation: 490 nm, Emission: 510-570) of the bound FAM-labeled aptamer previously dissociated from the surface of nanoparticles. After centrifugation at 13500 rpm for 15 min, at 4°C , the quantity of bound aptamer was determined with fluorescence (Excitation 490 nm, Emission 510-570 nm) at a Promega Glomax Multi-detection system. The concentrations of the aptamers were evaluated using a fluorescence standard calibration curve for standard solutions of the thrombin aptamer (**Figure 18:b**).

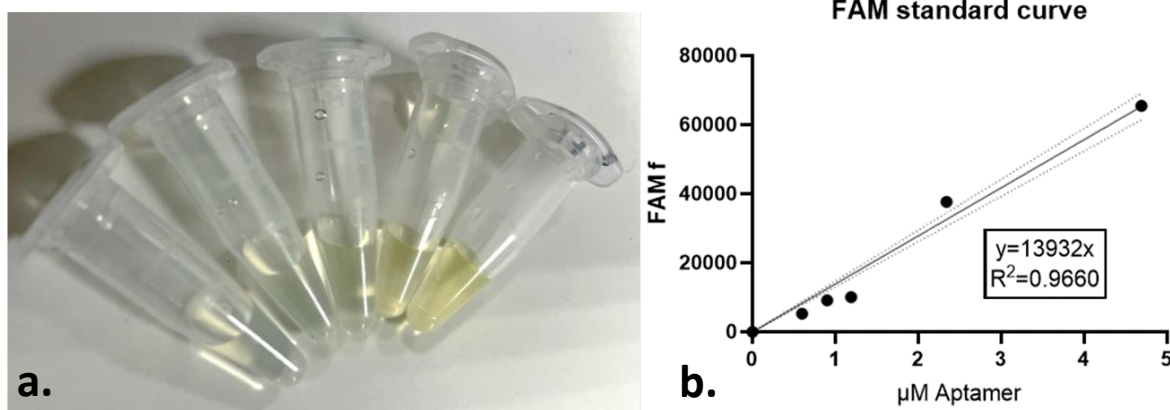


Figure 18: (a) 6-Carboxyfluorescein (FAM)-modified thrombin aptamer solutions in Tris-EDTA (TE) buffer (From left to right: 0.6, 0.9, 1.19, 2.34, 4.69 μM). (b) Standard curve of the fluorescence of FAM-modified aptamers (Excitation 490 nm, emission 510-570 nm).

¹²² Liu, B., Liu, J., [Methods for preparing DNA-functionalized gold nanoparticles, a key reagent of bioanalytical chemistry](#). Anal. Methods 9, 2633-2643 (2017).

The different employed concentrations of aptamers, which were utilized led to well-dispersed AuNPs' solutions after freezing, with an intense reddish color, as shown in **Figure 19:a** (tubes 2-6). On the other hand, the AuNPs that were frozen in the absence of aptamers aggregated, appearing greyish and were unable to resuspend (leftmost tube in **Figure 19:a**). The aptamer-AuNPs' suspension was stable even after 14 days, at 4°C, while AuNPs that were not modified with the thrombin aptamer aggregated at the bottom of the tube (**Figure 19:b**).

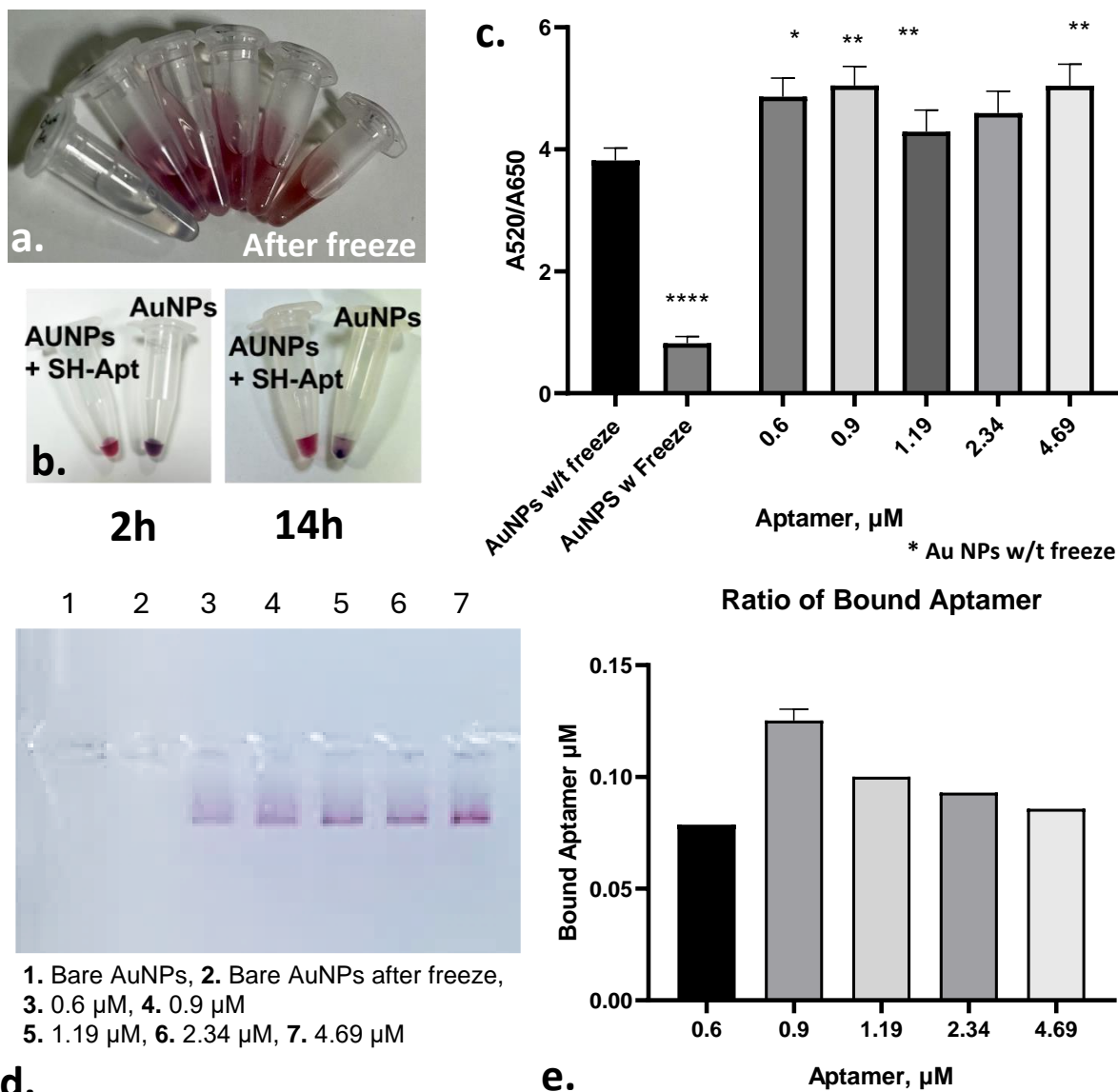
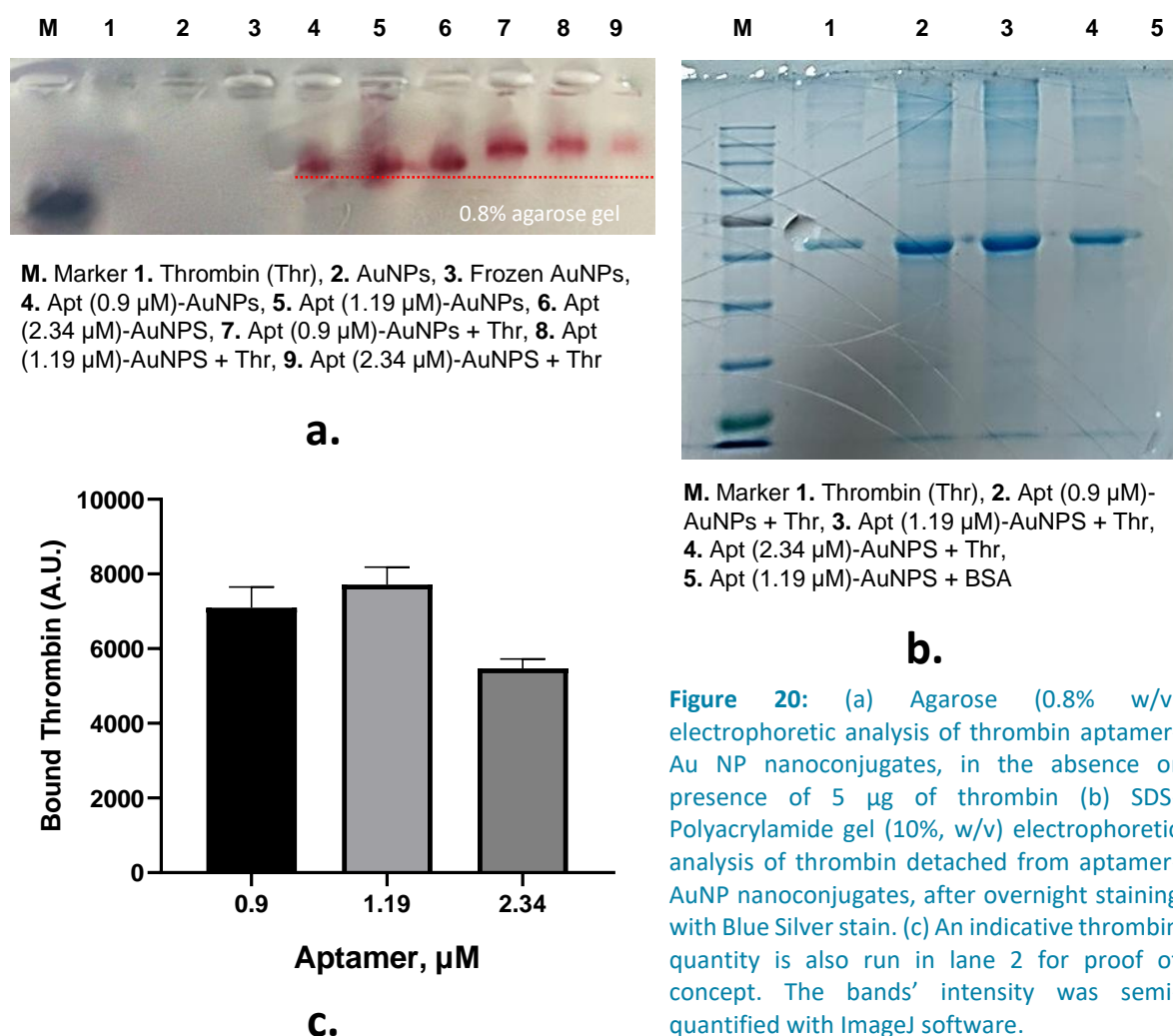


Figure 19: (a) Suspensions of Au NPs after freeze-thaw treatment, in the absence (far left tube) or presence of various concentrations of thrombin aptamer (From left to right: 0.60, 0.89, 1.19, 1.77, 2.34 μM). (b) Stability of AuNPs with freeze-thaw treatment in the absence or presence of aptamer, after 2 hours and 14 days. (c) The ratio of the absorbance of AuNPs' suspensions at 520 nm versus the one at 650 nm, before (w/t) and after (w) freeze-thaw treatment, and in the presence of several thrombin aptamer concentrations (0.60, 0.9, 1.19, 1.77, 2.34, 3.47 μM). (d) Agarose (0.8% w/v) electrophoretic analysis of AuNPs after freeze-thaw treatment in the absence or presence of various thrombin aptamer concentrations. (e) Number of thrombin aptamer molecules per AuNP after freeze-thaw treatment, detachment of aptamers with DTT and fluorometric analysis of 6-FAM. The concentration of the detached aptamers was calculated from a fluorescence standard curve (**Figure 18:b**).

To verify the effect of aptamer conjugation on AuNPs' stability, the ratio of absorbance at 520 nm versus the absorbance at 650 nm was also determined (**Figure 19:c**). An increase in this ratio coincides with increased dispersion of the nanoconjugates, while a decreased ratio is correlated with aggregation. Indeed, the conjugation with thrombin aptamer led to an increased stability of AuNPs' suspensions. On the contrary, when no aptamer is added, an abrupt decrease of the ratio A520/A650 was verified, as expected due to AuNPs' aggregation.

To further verify the conjugation of aptamers on AuNPs, aptamer-AuNP nanoconjugates were analysed with agarose gel (0.8% w/v) electrophoresis (**Figure 19:d**). The modification induced by the conjugation of the aptamer on AuNPs causes a shift in the motility of the samples through the agarose gel. The greater the amount of the aptamer conjugated, the more significant the up shift in motility was observed. In addition, the conjugated aptamer was detached from the AuNPs with DTT treatment and was determined with fluorometric analysis.

As shown in **Figure 19:e**, the highest fluorescence intensity of bound aptamer on AuNPs was obtained when 0.9 μM of aptamer was used. The average number of aptamers bound on the surface per AuNP was found by dividing the concentration of aptamers bound on the surface by the concentration of the gold nanoparticles used in conjugation being in good agreement with relevant literature.¹²²



A small decrease in the number of the attached aptamer molecules is verified at ratios above 1.19 μM of the employed aptamer, which may be due to stereochemical hindrance phenomena.

The greater the amount of the aptamer conjugated, the more significant the up-shift in motility was observed. In addition, the conjugated aptamer was detached from the Au NPs with DTT treatment and was determined with fluorometric analysis.

The efficiency of thrombin attachment on the modified AuNPs was evaluated using an SDS-PAGE technique. Different dilutions (0.6, 0.9, 1.19, and 2.34 μ M) of SH- modified thrombin aptamers conjugated to AuNPs were incubated with 5 μ g of human thrombin in TE buffer. The reaction was carried out in RT in the dark for 1 hour. To detect the specificity of aptamer-AuNP nanoconjugates to capture thrombin was evaluated using negative control samples with BSA protein. The conjugated thrombin on these AuNPs, the negative control samples, the bare AuNPs, and a standard human thrombin sample were loaded on a 0.8% agarose gel, and after running, an up-shift reflecting in reduced motility of the AuNPs, was verified, implying the binding of thrombin on the nanoconjugates (**Figure 20:a**). Subsequently, after detaching thrombin from the nanoconjugates samples were also loaded and run on a 10% Tris SDS-polyacrylamide gel (**Figure 20:b**). A standard human thrombin sample and a negative control (lane 1 and 5 respectively) were also loaded. After electrophoresis for 1 h, the gel was stained overnight with Blue Silver Stain to measure the intensity of bound protein using Image J Software (**Figure 20:c**). The analysis proved that nanoconjugates with a ratio of aptamer/AuNPs equal to 0.9 or 1.19 μ M possess similar thrombin binding activity. The ability to bind thrombin was found to reduce at a ratio of 2.34 μ M, which may be attributed to reduced aptamer density, as determined and shown in **Figure 19:e**.

c. Assessment of thrombin binding to TBA1-MNPs

Thrombin aptamer-MNPs were allowed to interact with either 5 μ g of thrombin, or BSA protein as a negative control marker. The mixture was incubated at RT for one hour with shaking, ensuring the reaction was protected from light to prevent photodegradation. After the incubation, the samples were centrifuged, and the supernatants were discarded.

The pellets were washed with HEPES 5mM (pH 7.6) containing 0.1% (w/v) BSA, to remove any unbound thrombin. Centrifugation and washing steps were repeated three times. Subsequently, samples were resuspended in TE buffer with 0.1% SDS, ensuring the final volume is twenty microliters so that the complex is fully immersed in the SDS solution.

This mixture was heated at 95°C for 30 min., a crucial step to detach the bound protein from the AuNPs-aptamer complex. Once the heating was completed, the samples were allowed to cool to RT. Electrophoresis loading buffer was added to the samples, and then the samples were loaded onto an SDS-PAGE (10% w/v) for further analysis. After the gel run, staining of protein bands was performed with Blue Silver staining and destaining with d.d. H₂O.

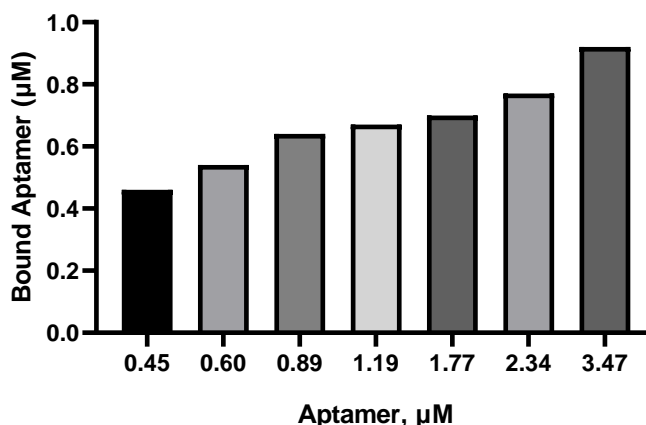
Preliminary results with TBA1 aptamer on core-shell NPs provide promising results (**Figure 21:**), proving successful conjugation of TBA1 on magnetite core-shell NPs and subsequent positive binding of thrombin. Freeze-thaw treatment of NPs in the presence of aptamer retained the burgundy-like color of the NPs, while in the absence of TBA1, the color of the NPs turned to brownish (**Figure 21:a**). In addition, bound aptamer was increased linearly when employing increasing initial aptamer concentration (**Figure 21:b**).

Finally, when the nanoconjugates were mixed with thrombin, decreased electrophoretic motility was verified (**Figure 21:c**), proving successful interaction of TBA1-NPs with thrombin. Extensive experimental analysis is currently underway to verify and optimize the received experiments. The detailed protocol of the conjugation methodology is summarized in **Table 6**.

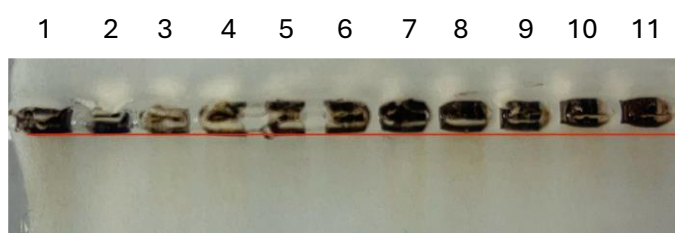


a.

Figure 21: (a) Suspensions of core/shell NPs after freeze-thaw treatment, in the absence (far left tube) or presence of various concentrations of thrombin aptamer (From left to right: 0.60, 1.19, 2.34, 3.47 μM). (b) Bound thrombin aptamer on core/shell NPs after freeze-thaw treatment, detachment of aptamers with DTT, and fluorometric analysis of 6-FAM. The concentration of the detached aptamers was calculated from a fluorescence standard curve (Fig. 1b). (c) Agarose (0.8% w/v) electrophoretic analysis of thrombin aptamer-core/shell NP nanoconjugates, in the absence or presence of 5 μg of thrombin (1->11: pure core-shell Au NPs; core-shell Au NPs with 0.60, 1.19, 2.34, 3.47 μM of TBA1 aptamer; core-shell Au NPs with 0.60, 1.19, 2.34, 3.47 μM of TBA1 aptamer, and after incubation with 5 μg of thrombin).



b.



c.

Table 6: Overview of the aptamer-nanoparticle conjugation

Nanoparticles	Aptamer	Target Protein
Gold NPs	TBA1 (5'-GTTGGTGTGGTTGG-3')	Thrombin
Core Shell NPs	TBA1 (5'-GGTGGTGTGGTTGG-3')	
Outcomes	<ol style="list-style-type: none"> Efficient conjugation of TBA1 on nanoparticles. Protected complex from precipitation after freezing. Stable complex for at least 2 weeks 	
Method of Conjugation	NPs are mixed with SH-Aptamer (0.6 μM , 0.9 μM , 1.19 μM , 2.34 μM , 4.69 μM) at a final volume of 500 μl . The tubes were kept at -20°C for at least 2 hours and then thawed at RT. Aptamer- NPs were washed three times with Tris-EDTA buffer, pH 8 (TE) and centrifuged to discard the unbound aptamers at 13.500 rpm, for 15 min, at 4°C .	

Consequently, we have proved that the proposed methodology was adequate for conjugating Au NPs nanoparticles with active thrombin aptamer. Thrombin, an activating protease of multiple receptors, is implicated in some vascular diseases, including AD. The employment of aptamers in combination with traditional methods and magnetic nanomaterials, strengthens the sensitivity of thrombin detection. These results are promising for our immediate next goals, which are i) the validation of the conjugation with additional analytical specialized protocols and ii) the application of the protocol in other AD hallmarks, e.g. amyloid beta peptides, tau protein.

2.5 Future steps

Progress towards the 2D-BioPAD targets (i.e., Key Performance Indicators) for the AD biomarkers studied so far is as follows:

AI: We have narrowed down how to translate the indicative aptamers to contribute to a better experimental development, following literature model metrics.¹²³ Alternative protein sequences are examined, as potential new aptamer candidates with good. Results expected within this semester.

NFL: Selection and sequencing for NFL are completed and the NGS data obtained is being analysed to obtain information about motifs, clusters and secondary structure. The quality parameters such as, pool PCR amplification, single-stranded DNA generation are satisfactory and within the next few months will proceed in Task 2.2 on the functionalization of NFL aptamers according to the initial schedule.

GFAP: Selection and bio-informatic analysis of the selected pools are completed. Pools were well and progressively enriched under the applied selection pressure we are currently working on Task 2.2 on the functionalization of GFAP aptamer according to initial schedule.

A β 40 and A β 42: As literature aptamers' binding was inconclusive, we plan to launch a new selection based on discussions with Steering committee members, clinical partners and external experts. The selection process is expected within the next semester. We are currently examining the conjugation of commercially available aptamers: for AB40, RNV95¹²⁴ (previously described as suitable aptamer for use in a wide range of affinity assays to detect low-molecular-weight A β 40 oligomers)¹²⁵ and A β 7-92-1H1¹²⁶ (previously described to possess high specificity for the A β 42 monomer).¹²⁷ Besides the poor outcome of the experiments performed at Novaptech, conjugation experiments of these aptamers with the synthesized MNPs and amyloid peptides are regarded as useful for future reference, as these aptamers were generally regarded acceptable in the literature for targeting amyloid peptides. The performance of these aptamers will be evaluated with the involvement of sophisticated immunological techniques (Western blotting, commercial ELISA kits, Dot blotting) in combination with specific antibodies for amyloid peptides β -Amyloid (1-42) (D9A3A) Rabbit mAb #14974 and β -Amyloid (1-40) (D8Q7I) Rabbit mAb Cell Signaling Technology).¹²⁸

pTau217, pTau231 Commercial availability issues. The required quantity and desired form of protein are not available commercially. Contact with external partners to provide targets is underway. After aptamer design, the further steps will be the employment of specific antibodies for Tau (D1M9X) XP Rabbit mAb (#46687, Cell Signaling Technology) and for Phospho-Tau (Thr231) (#71429, Cell Signaling Technology), to prove the specific binding with the corresponding protein.

The next steps involve fine-tuning the synthesis parameters to exert precise control over the size of the nanoparticles, in their core and shell dimensions. This adjustment will enable us to tailor the properties of the nanoparticles to better suit our intended applications in biomarker binding and quantitative analysis. Additionally, further structural and magnetic characterization of the samples is

¹²³ Shin I. et al. [AptaTrans: a deep neural network for predicting aptamer-protein interaction using pretrained encoders](#) *BMC Bioinformatics* 24:447 (2023).

¹²⁴ 5'-TGGGGGGCGGACGATAGGGGCCCGGTAGGATGGACG-3'

¹²⁵ Chakravarthy M et al. [Development of DNA aptamers targeting low-molecular-weight amyloid- \$\beta\$ peptide aggregates: In vitro](#) *Chem Commun* 54:4593–4596 (2018).

¹²⁶ 5'-CCGGTGGGGGACCACTACAAAAGTGGGTAGGGCGGTTGGAAAA-3'

¹²⁷ Zheng Yet al., [Development of DNA Aptamer as a \$\beta\$ -Amyloid Aggregation Inhibitor](#). *ACS Appl Bio Mater.* 3, 12, 8611–8618 (2020).

¹²⁸ This rabbit monoclonal antibody specifically recognizes the human A β 42 isoform. The conjugation of A β 7-92-1H1 to A β 42 can be detected using Western Blot and/or ELISA methods with this antibody. This antibody will be used after the detachment of A β 42 peptide from its corresponding aptamer, in order to prove that RNV95 binds specifically the A β 40 peptide.

planned. This comprehensive analysis will provide deeper insights into the composition, morphology, and magnetic behavior of the synthesized nanoparticles. By delving into these aspects, we aim to elucidate the relationships between synthesis parameters and nanoparticle properties, thereby optimizing the synthesis approach for enhanced electrochemical performance.

3. Interactions

The selected aptamers will also be tested in the presence of other similar proteins and more complex solutions with known concentrations of the selected biomarkers. Moreover, we will also determine the low detection limit (LOD), the lowest concentration of the selected biomarkers that our aptamers can detect. A LOD of 0.25 fM has been achieved with previous biosensors detecting amyloid beta 1-42, thus an equal or better LOD should be achieved. Possible redesign and optimization might be needed after the first testing. Immobilization on NPs might change the binding capacity and specificity of the aptamers. Thus, it is essential to use our results as input for optimization of the final product before the involvement of graphene (WP3). Towards achieving our goal of high sensitivity and specificity, all tasks of WP2 should be jointly and in constant communication with elements of resilience in our innovative design.

Key to advanced graphene biosensors is the tailored, reproducible chemical functionalization of the graphene surface. This functionalization is crucial for the effective and selective recognition of target analytes, enhancing signal generation, selectivity, and sensitivity. Graphene derivatives are highly promising for chemical and biochemical sensors, particularly in electrochemical and field-effect transistor (FET) devices enhancing electron transfer between the biorecognition site and the electrodes, improving the signal-to-noise ratio, and boosting the selectivity and sensitivity of the devices.¹²⁹ Furthermore, graphene derivatives can also be integrated with other materials to tackle similar challenges.¹³⁰

Different chemistry will be exploited in order to attach the DNA on graphene-derivatives and nanocomposites. As a result, a signal increase will be achieved only in the presence of the target, due to the hybridization event between the capture strands immobilised on the electrodes and the DNA strands tagged with MB. Different electrochemical techniques will be investigated (i.e., square wave voltammetry and impedance).

The paper-based sensing device leverages the intrinsic passive microfluidic properties of paper to facilitate the movement of liquids. This natural characteristic of paper allows it to wick and transport fluids such as buffers and electrolytes efficiently without requiring any external pumps or power sources. When a sample is applied to the paper, the capillary action inherent to the paper's fibrous structure ensures that the liquid spreads evenly across the substrate, effectively "wetting" the paper with the necessary reagents for the electrochemical measurements.

This passive microfluidic action is crucial for the initial stages of the assay, where it ensures that the paper is adequately saturated with the buffer solution and electrolyte. This saturation is essential for maintaining the proper ionic environment necessary for accurate electrochemical measurements. By relying on the passive flow, the device simplifies the operation, making it user-friendly and suitable for point-of-care applications where simplicity and reliability are paramount.

In addition to the passive microfluidic mechanism, the device incorporates active control of the flow using magnetic fields to manipulate aptamers conjugated with magnetic nanoparticles. This magnetic control plays a critical role in enhancing the overall assay performance. During the incubation phase, the external magnetic field ensures that the magnetic nanoparticles, which are functionalized with aptamers, remain concentrated in the vicinity of the target biomarkers. This focused interaction

¹²⁹ Flauzino, J. M. R. et al. [Label-Free and Reagentless Electrochemical Genosensor Based on Graphene Acid for Meat Adulteration Detection](#) Biosensors and Bioelectronics, 195, 113628 (2022).

¹³⁰ Palley, B. F. et al., [Electrochemical Biosensors Composed of Polyethylenimine \(PEI\) and Graphene Derivatives for Rapid Detection of Alzheimer's Disease](#) Meet. Abstr. MA2023-02 3006 (2023).

increases the likelihood of binding events, thereby improving the capture efficiency of the target molecules.

Once the incubation is complete, the magnetic field is used to transport the nanoparticles to the detection zone where the graphene electrodes are located. This precise movement ensures that the captured biomarkers are effectively brought into contact with the functionalized electrodes, enabling highly specific and sensitive electrochemical detection. The use of magnetic manipulation allows for greater control over the assay conditions, ensuring that the target molecules are optimally positioned for detection. Currently, synthesized NPs are sent and being studied in ICN2.

Following the detection phase, the magnetic nanoparticles are guided to the absorbent pad. This step is essential for the cleaning process, as it helps to remove unbound and non-specifically bound molecules from the detection area. By directing the nanoparticles to the absorbent pad, the device minimizes background signals and reduces non-specific binding, thereby enhancing the accuracy and reliability of the sensor.

ICN2 will work on the control of nanoparticles with magnetic properties to enable real-time movement and positioning as well as performing electrochemical measurements. To achieve this, a device capable of interacting with the magnetic properties of the particles will be developed, along with software to control it. This document outlines the expected operation of the software and specifies the functional and non-functional requirements anticipated for the system, while allowing for the possibility of future requirements.

The software will be developed as a smartphone application for both iOS and Android platforms. This application will control the movement of the nanoparticles through a magnetic actuator system and measure variations with a sensor to determine the position of the particles.

To control movement, the system can activate, deactivate, or invert the magnetic field multiple times as needed to induce motion. Additionally, it will be necessary to control the intensity, frequency, and duration of the magnetic field. Position control of the particles is a primary objective, so the system must continually locate the particles, save this data, and allow the user to view it.

Our application will be designed for non-technical personnel, presenting a simple and intuitive interface. However, it must also provide researchers with more precise control, necessitating two different interfaces and a mechanism to differentiate users according to their roles.

Finally, the application will connect to the physical device using NFC (Near Field Communication) potentiostat, which operates at short distances for the electrochemical measurements. Data will be stored in a European hub, enabling data exchange.

The mobile app will feature a comprehensive Digital User Guide designed to assist HCPs in effectively utilizing the device. To continuously improve the device and the mobile app experience, a dedicated feature for HCPs to provide feedback will be integrated into the app. This feature will allow HCPs to share their experiences, report any issues, and suggest enhancements directly through the app. Feedback submission will be straightforward, with a designated section accessible from the main menu.

4. Conclusions

The activities conducted under WP2 of the 2D-BioPAD project, focusing on the identification, synthesis, and evaluation of aptamers for AD protein biomarkers and the synthesis and characterization of magnetic nanoparticles (MNPs) as carriers, have made significant progress. Key conclusions from this reporting period are:

1. Progress in Aptamer Identification:

- Task 2.1 has made strides in the identification of DNA aptamers specific to key AD biomarkers, including A β 40, A β 42, NF-L, GFAP, and p-tau 217. This task is still ongoing, with further work required to finalize the selection of aptamers for these protein biomarkers. The progress so far sets a strong foundation for subsequent tasks.

2. Readiness for Subsequent Tasks:

- The successful progress in Task 2.1 is critical as it serves as a prerequisite for the initiation of Task 2.2, which will focus on the optimization and functionalization of these aptamers. The finalization of aptamer identification will trigger the next phase, which involves synthesis and optimization.

3. Synthesis and Characterization of Magnetic Nanoparticles:

- Objective 2.2 has been partially fulfilled with the synthesis of MNPs. Characterization of these nanoparticles is still ongoing and is expected to be completed in the next reporting period. This work is crucial for ensuring the MNPs can effectively act as carriers and enablers in conjunction with the selected aptamers.

4. Conjugation and Validation Processes:

- Preparatory work for Objective 2.3 has begun, with initial formulations of MNPs being prepared for conjugation with the aptamers identified in Task 2.1. Full achievement of Objective 2.3 is anticipated by the end of WP2, contingent on the successful conclusion of ongoing tasks.
- Task 2.4 has started preliminary evaluations and validations of the conjugated MNPs and aptamers, establishing protocols that will guide future experimental work.

5. Iterative Aptamer Selection Process:

- The selection of aptamers is a complex, iterative process that involves multiple rounds of incubation and selection. This iterative nature is on-going ensuring that only the most effective aptamers are selected for further development, although it also means that progress in this area is necessarily gradual.

6. Foundational Work for Future Research:

- The work done in this period lays the groundwork for WP3, where the identified aptamers and characterized MNPs will be integrated into a graphene-based sensing platform. This upcoming work is essential for developing the standardized nano-based probes aimed at early AD diagnosis.

Overall, WP2 is on track, with key milestones being met. Continued efforts in aptamer identification and MNP characterization will be crucial for the successful achievement of WP2's objectives and for paving the way for subsequent work packages in the project.



Supple Graphene Bio-Platform for point-of-care early detection and monitoring of Alzheimer's Disease

GA 101120706

Partners



Follow us

